Available online at www.sciencedirect.com
ScienceDirect
Geochimica et Cosmochimica Acta 71 (2007) 335–353
Geochimica
www.elsevier.com/locate/gca

Origin of convex tetrads in rare earth element patterns of hydrothermally altered siliceous igneous rocks from the Zinnwald Sn–W deposit, Germany

T. Monecke [a,*], P. Dulski [b], U. Kempe [c]

[a] Department of Earth Sciences, University of Ottawa, Marion Hall, 140 Louis Pasteur, Ottawa, Ont., Canada K1N 6N5
[b] GeoForschungsZentrum Potsdam, Telegrafenberg, D-14473 Potsdam, Germany
[c] Institute of Mineralogy, TU Bergakademie Freiberg, Brennhausgasse 14, 09596 Freiberg, Germany

Received 12 April 2006; accepted in revised form 5 September 2006

Abstract

The chondrite-normalized rare earth element (REE) patterns of whole rock samples from evolved granitic systems hosting rare metal deposits sometimes show a split into four consecutive curved segments, referred to as tetrads. In the present contribution, a rigorous statistical method is proposed that can be used to test whether geological significance should be attributed to tetrads that are only of limited size. The method involves a detailed evaluation of element and sample specific random and systematic errors that are constrained on the basis of independent repeated preparations and analyses of sample and reference materials. Application of the proposed method to samples from the granite-hosted Zinnwald Sn–W deposit, Germany, revealed that at least two tetrads in normalized whole rock REE patterns have to be analytically significant to rule out that fractional crystallization led to the unusual behavior of the REEs. Based on the analysis of altered albite granite and greisen samples from the endocontact of the Zinnwald granite massif, it is demonstrated that the lanthanide tetrad effect is responsible for the formation of the convex tetrads. Geological and petrological evidence suggests that the tetrads in the samples developed prior to greisenization and related cassiterite precipitation. In contrast to the endocontact samples, the rhyolitic wall rocks are typified by normalized REE patterns having tetrads that are variable in size and frequently close to the limit of analytical significance. The sizes of the tetrads apparently correlate with the intensity of albitization, but show no relation to subsequent alteration processes including greisenization and low-temperature argillization. This observation proves that curved segments in normalized whole rock REE patterns can be introduced during hydrothermal fluid–rock interaction.

1. Introduction

In the past decades, the geochemical behavior of the rare earth elements (REEs) has been studied extensively because this group of elements provides a range of geochemical indicators that can be used to constrain the evolution of magmatic and hydrothermal systems (e.g., Möller and Muecke, 1984; Masuda and Akagi, 1989; Raimbault et al., 1993; Dostal and Chatterjee, 1995; Bau, 1996; Pan and Breaks, 1997; Möller, 1998; Irber, 1999; Monecke et al., 2000). It has been shown that variations in the geochemical behavior of the REEs primarily result from differences in their ionic radii (ionic radii of the REEs decrease steadily with atomic number) as well as variations in valence states (Ce^{3+} and Ce^{4+}, Eu^{2+} and Eu^{3+}). An additional feature that potentially influences the distribution of the REEs in some geological environments is the lanthanide tetrad effect (Masuda et al., 1987; Kawabe, 1995; Bau, 1996; Irber, 1999; Monecke et al., 2002). This effect causes a split of the normalized REE patterns into four consecutive curved segments that are referred to as tetrads (first tetrad: La–Ce–Pr–Nd; second tetrad: (Pm)–Sm–Eu–Gd; third tetrad: Gd–Tb–Dy–Ho; fourth tetrad: Er–Tm–Yb–Lu). The tetrads are either convex or concave forming M- and W-shaped lanthanide patterns, respectively (Masuda et al., 1987).

* Corresponding author. Fax: +1 613 562 5848.
E-mail address: tmonecke@uottawa.ca (T. Monecke).

0016-7037/$ - see front matter © 2006 Elsevier Inc. All rights reserved.
doi:10.1016/j.gca.2006.09.010

Several investigations have established that whole rock samples from evolved granitic systems, frequently hosting rare metal deposits, may exhibit convex tetrads (Masuda and Akagi, 1989; Cocherie et al., 1991; Förster and Tischendorf, 1994; Lee et al., 1994; Kawabe, 1995; Bau, 1996; Irber, 1999; Jahn et al., 2001; Monecke et al., 2002; Takahashi et al., 2002; Takahashi and Kawabe, 2003).

A number of early studies have suggested that curved segments in the REE patterns of whole rock samples from evolved granitic systems form during magmatic crystallization due to selective incorporation of the REEs into fractionating accessory phases (Yurimoto et al., 1990; Zhao and Cooper, 1993; McLennan, 1994; Pan, 1997; Pan and Breaks, 1997). Yurimoto et al. (1990) proposed that the discontinuity between Nd and Sm may be caused by the fractionation of monazite and Pan (1997) showed that a similar break between Ho and Er may form in response to the crystallization of garnet. However, subsequent studies by Bau (1997) and Irber (1999) demonstrated that the exact shapes and sizes of tetrads cannot be correctly reproduced by Rayleigh model calculations and that whole rock REE patterns with more than one rounded segment can only be obtained assuming unrealistic mineral assemblages. Furthermore, accessory minerals including garnet, monazite, xenotime, and apatite typically have REE patterns with tetrads similar to the related granitic rocks (Förster, 1998; Irber, 1999; Masau et al., 2000; Kempe and Götze, 2002) ruling out the possibility that whole rock samples acquire convex tetrads during fractional crystallization.

Kawabe (1995), Irber (1999), and Dolejš and Štemprok (2001) proposed that the development of convex segments in whole rock REE patterns is caused by processes of fluid-melt interaction during crystallization of the silicate melt under open system conditions whereby a complementary REE pattern with concave tetrads is removed from the solidifying magma by coexisting (or exsolved) hydrothermal fluids. This model was found to be inconsistent with subsequent observations by Monecke et al. (2002) demonstrating that hydrothermal precipitates also show REE patterns with convex tetrads. Hydrothermal fluids derived from the granite magma are, therefore, unlikely to remove complementary REE patterns with concave tetrads from the solidifying melt.

A third model for the development of convex tetrads in the REE patterns of granitic rocks has been proposed by Masuda and Akagi (1989) and, more recently, by Takahashi et al. (2002). These authors suggested that a complementary REE pattern with concave tetrads is removed during surface weathering. The evidence supporting the development of tetrads in response to weathering has been questioned by Monecke et al. (2003).

Recent investigations have demonstrated that advances in this field can only be made by quantifying the sizes of the tetrads and correlating them with other geochemical, mineralogical, and petrographic indicators (Irber, 1999; Monecke et al., 2002; Takahashi et al., 2002). However, this approach is limited by the fact that normalized REE patterns of granitic rocks frequently possess tetrads that are only small in size. In the case of such subtle tetrads, a clear distinction between analytically significant curvatures and analytical artifacts is tenuous (McLennan, 1994). In a given sample suite, small, but geochemically significant, differences in the tetrad sizes may be difficult to distinguish from variations introduced by the random errors of the REE determinations. Consequently, geochemical interpretation and correlation of the sizes of subtle tetrads with other indicators is typically precluded even if the REE measurements were performed at reasonable precision and accuracy (McLennan, 1994; Monecke et al., 2003; Takahashi et al., 2003).

In the present contribution, an analytical procedure is presented that has been developed to allow a distinction of subtle tetrads from analytical artifacts. The developed method involves a rigorous evaluation of random and systematic errors that are constrained by repeated independent preparation and analysis of reference materials and samples. In contrast to earlier studies, it is taken into account that random errors are element specific and have to be determined individually for each sample. As an example, the proposed method has been applied to whole rock samples from the granite-hosted rare metal deposit Zinnwald, Germany, that show variable tetrad sizes. Based on the careful error evaluation, it is critically assessed to what extent analytical uncertainties are able to account for subtle tetrads. Implications to the understanding of the geochemical processes involved in the development of tetrads in whole rock REE patterns of granitic rocks are discussed.

2. Geological setting

The Zinnwald deposit is a Sn–W deposit located in the Erzgebirge region, Germany, which represents the eastern part of the Herzynian tin province. The deposit occurs at the border between Germany and Czech Republic and represents, geologically, the northern continuation of the Cínovec deposit that is located to the south on the territory of Czech Republic (Fig. 1). The deposit is mainly hosted by a small, highly evolved Li–F granite massif that has an elliptical shape at surface (1.4 by 0.3 km in plan view). The contact between the Zinnwald granite and the surrounding rhyolitic wall rocks has a shallow outward dip, except for the western contact that is very steep. The rhyolite belongs to the Teplice volcanic complex (Štemprok, 1967; Štemprok and Šulcek, 1969; Ďurišová et al., 1979).

The Zinnwald granite massif is internally complex. Various petrographically distinct granite types have been observed. The upper portion of the granite massif is dominated by Li-rich zinnwaldite-bearing albite granite that passes at depth into Li-poor protolithionite-bearing granite. Deep drilling revealed that the transition between both granite types is gradational and occurs at a depth of ~730 m from surface (Štemprok and Šulcek, 1969; Cocherie et al., 1991; Johan and Johan, 1994). Recent investigations have shown that the upper Li-rich zinnwaldite-bearing al-

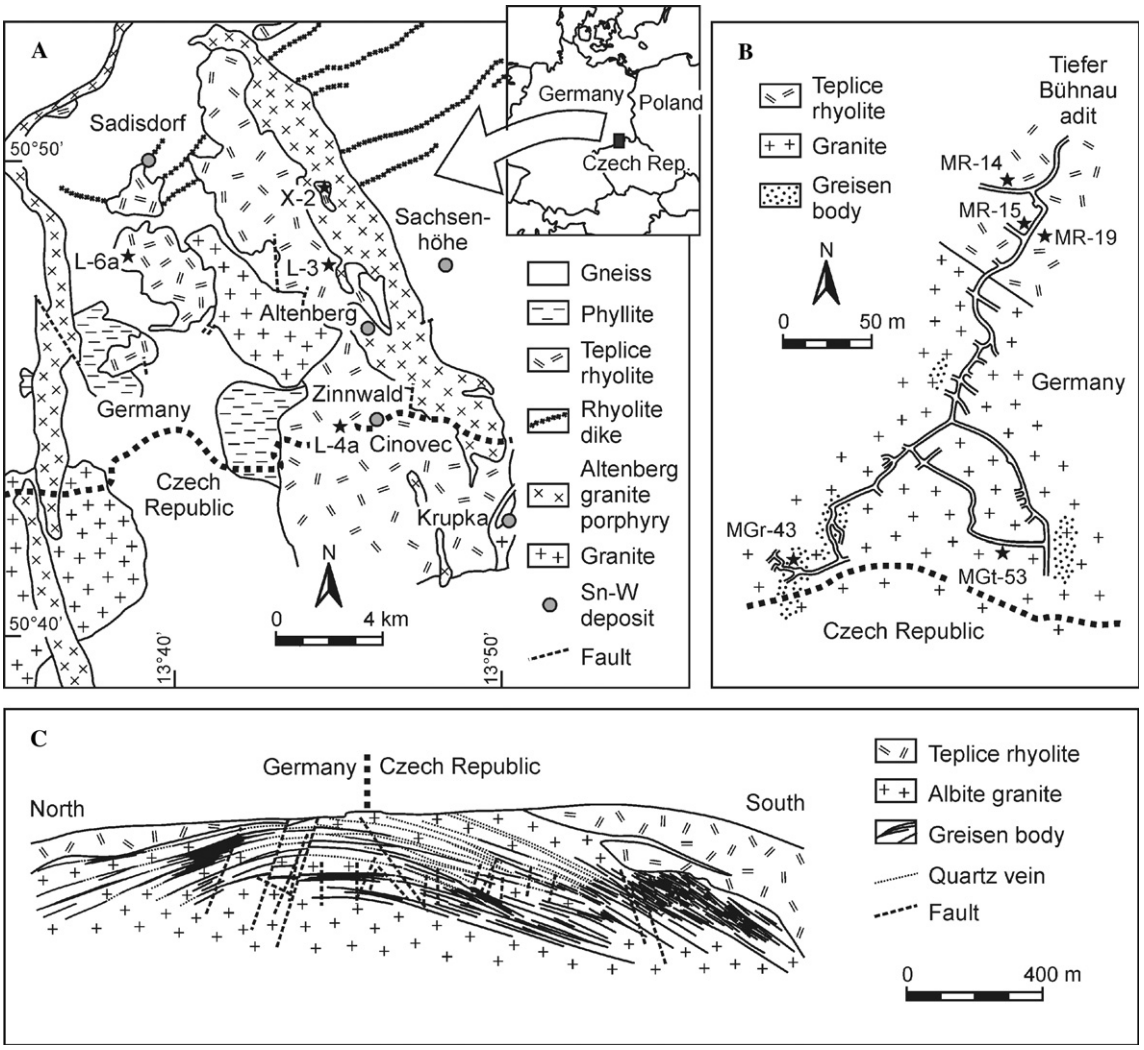

Fig. 1. Sample locations of the variably altered endo- and exocontact rocks from the Zinnwald deposit and surroundings: (A) Simplified geological map of the eastern Erzgebirge showing the distribution of granite-associated Sn–W mineralization and the occurrence of the Teplice rhyolite. All Sn–W deposits shown are spatially associated with small stocks of evolved granite intrusions, (B) plan view of the Tiefer Bühnau adit (modified from Sala, 1999), and (C) simplified geological section through the Zinnwald deposit (modified from Štemprok et al., 1995).

bite granite contains zones of Li-rich lepidolite-bearing albite granite (Rub et al., 1998; Sala, 1999). Microgranitic intercalations of variable thicknesses have been observed in the upper Li-rich zinnwaldite-bearing albite granite and the lower Li-poor protolithionite-bearing granite (Štemprok and Šulcek, 1969; Ďurišová et al., 1979; Webster et al., 2004). In addition, granitic dikes with evolved geochemical signatures are present in the exocontact (Webster et al., 2004).

The Sn–W mineralization is confined to cassiterite–wolframite–quartz veins and large greisen bodies (Cocherie et al., 1991). Mineralized veins occur largely in the upper 220 m of the granite massif (Fig. 1), but are also present in the surrounding rhyolitic wall rocks. Two types of veins can be distinguished, namely flat-lying, up to 4 m thick and intensely mineralized veins with a centroclinal strike, and steeply dipping quartz veins that also carry some Sn mineralization. Detailed underground mapping by the authors revealed that the flat-lying veins postdate the steeply dipping veins (note that the steeply dipping veins have been reactivated during hydrothermal activity postdating the formation of the flat-lying veins). The large greisen bodies carried the most significant Sn mineralization at Zinnwald. The bodies are restricted to the endocontact of the granite intrusion and occur mainly near the eastern and western contacts to the rhyolite (Fig. 1). The greisen bodies consist largely of quartz, zinnwaldite, lepidolite, and topaz. They are steeply dipping and pipe-shaped, but transform to flat-lying bodies near the intersections with the flat-lying quartz veins, resulting in overall highly irregular shapes. The root zones of the greisen bodies can be traced to at least 1200 m depth (Webster et al., 2004). Away from the large greisen bodies, greisenization extends along the selvages of the cassiterite–wolframite–quartz veins (Štemprok and Šulcek, 1969). The field evidence suggests that greisenization postdated flat vein formation. In addition to endocontact greisen bodies,

cassiterite-bearing greisen stringers are present in the exocontact.

Polyphase formation of the Sn–W mineralization was accompanied by complex hydrothermal alteration of the granite resulting in intense alteration of endocontact rocks. Field observations and microscopic investigations have established that the hydrothermal alteration postdated the solidification of the granite (Štemprok, 1967; Sala, 1999). Early albitization is widespread throughout the entire granite massif. This type of alteration resulted in pronounced changes in the overall mineralogical and geochemical signatures of the granitic rocks. Albitization of the granite was postdated by high-temperature greisenization and the formation of the large greisen bodies. Greisenization associated with Sn mineralization resulted in the formation of early, extensive Li mica-bearing greisen bodies (Li-rich greisen type) and late, spatially more restricted, muscovite greisen veins and zones (Li-poor greisen type). The intensity of albitization and greisenization generally decreases with depth within the Zinnwald granite massif (Dolejš and Štemprok, 2001).

Various types of low-temperature alteration postdated formation of the ore. Particularly widespread, and spatially unrelated to the greisenization, is the development of an argillic alteration mineral association that is typified by the abundant presence of kaolinite (Štemprok, 1967; Štemprok and Šulcek, 1969), illite, fluorite, barite, and uranium phosphates.

The petrographic and petrological characteristics of the Teplice rhyolite hosting the Zinnwald granite have been studied by numerous workers including Wolf (1960), Lobin (1986), Seltmann and Breiter (1995), Seltmann et al. (1996), Breiter (1997), Štemprok et al. (2003), and Müller et al. (2005). The Teplice rhyolite forms a (possibly polyphase) ignimbrite body that covers the Proterozoic crystalline basement. The rhyolite has a thickness of up to ~2 km, an E–W extension of up to 8 km, and a maximum N–S extension of ~20 km with the Zinnwald deposit located in its southern portion (Fig. 1). Based on the relative abundance of crystals and crystal fragments as well as alteration characteristics, the Teplice rhyolite can be subdivided in a lower and upper part (Pälchen, 1968). Intense sericitization is widespread in the lower part of the Teplice rhyolite containing sparse crystals and crystal fragments whereas this style of alteration is rare or absent in the upper portion that is typified by a high content of crystals and crystal fragments. Alteration styles present in both parts of the Teplice rhyolite include albitization, greisenization, and argillization. Alteration is apparently most intensely developed around known Sn–W mineralization.

3. Sample selection

Sample selection for the present study was based on the findings of Monecke et al. (2002). These authors showed that granite and greisen samples from the Zinnwald granite massif are typified by REE patterns with relatively pronounced tetrads. However, calculation of the tetrad sizes revealed that only the first and third tetrads are significant from the analytical point of view (Monecke et al., 2002) hampering unequivocal interpretation of the REE patterns. To test whether all quantifiable tetrads are of geochemical significance if an improved analytical approach is used, one albite granite and a greisen sample have been selected for the present study (Fig. 1). Both samples were affected by intense hydrothermal alteration, but showed no evidence of surface weathering.

In addition to the two endocontact samples, several samples from the Teplice rhyolite have been selected. Previous investigations by Monecke et al. (2002) have shown that exocontact samples exhibit REE patterns with very subtle tetrads that were, at the time, found to be insignificant from the analytical point of view. To investigate the geochemical significance of these subtle tetrads in detail, seven altered rhyolite samples were taken from surface outcrops and underground exposures in the Tiefer Bühnau adit (Fig. 1). The samples were collected from the upper part of the Teplice rhyolite that is not affected by intense low-temperature sericitization. However, all samples show at least some evidence for hydrothermal alteration related to the formation of Sn–W mineralization. The samples were not affected by significant chemical surface weathering.

4. Analytical methods

Initially, the rock samples were studied in hand specimen. Representative thin sections were then prepared for petrographic inspection by optical microscopy and scanning electron microscopy (SEM). The SEM investigations have been conducted using a Jeol JSM 6400 microscope equipped with a Tracor (Noran) series II energy-dispersive X-ray spectrometer. Routine operating conditions were 20 kV with a beam current of 600 pA.

Subsequent to the petrographic inspection, the whole rock samples (3 kg sample material) were crushed and split with a riffle splitter. A split of approximately 300 g material was pulverized to analytical fineness using a centrifugal agate ball mill. The geochemical composition of the samples was constrained by a combination of analytical methods. The abundances of the major elements and the trace elements Rb, Sn, and Ba were established by conventional X-ray fluorescence analysis (XRF). The concentrations of F and Li were measured by ion specific electrode detection and flame atomic absorption spectrometry, respectively. The Cs and REE concentrations were determined by inductively coupled plasma-mass spectrometry (ICP-MS).

The REE concentrations of the pulverized whole rock samples were determined on specially prepared sample solutions by a method similar to that described by Dulski (2001). Initially, 100 mg aliquots of the finely powdered samples were dissolved by a mixed acid digestion ($HF/HClO_4$) in PTFE digestion vessels for 16 h under pressure at 180 °C. After cooling, the samples were evaporated to

near dryness, re-dissolved with 5 ml HCl (10 mol l^{-1}), and evaporated again at 180 °C to incipient dryness. The moist hot residues were taken up again by 5 ml HCl (10 mol l^{-1}) and, after closing the digestion system, treated at 130 °C for 12 h. After cooling, the solutions were again evaporated to incipient dryness and the hot sample cakes were then carefully re-dissolved in 2 ml HCl (10 mol l^{-1}) and 10 ml purified water (18 Ω resistivity). Final sample dissolution was performed with HCl because high field strength elements such as the REEs are stabilized in solution in this way (Münker, 1998; Robinson et al., 1999; Dulski, 2001). The resulting clear solutions were filled into 50 ml volumetric flasks, made up to volume with Milli-Q water and transferred into 50 ml polyethylene bottles. Prior to analysis, Ru, Re, and Bi were added to aliquots of the solutions as internal standards for drift correction, and the mixtures were diluted by a factor of ten. Solutions prepared according to the procedure described above show a dilution factor of 5000 and are about 0.5 mol l^{-1} in hydrochloric acid. Together with a batch of 14 samples, two procedure blanks were prepared using the same procedure.

The ICP-MS measurements have been performed using an externally calibrated ELAN 5000A quadrupole ICP mass spectrometer (Perkin-Elmer/SCIEX, Canada). The system was optimized to a sensitivity of approximately 80,000 cps for lanthanum and uranium in a 10 ng ml^{-1} tuning solution and a yield for CeO^+ formation of about 2%. The samples were analyzed in small batches comprising only 4–5 sample solutions and a quality control solution to monitor the instrumental drift. Each batch was preceded by a calibration solution (10 ng/ml of individual REE), two acid blanks, and a procedure blank. To correct for signal drift during each analytical run, Ru and Re were used as internal standards. Within one run, drift correction factors were calculated using ratios of the count rates of Ru and Re for the first solution relative to those in each solution measured. Interference corrections have been routinely applied to correct analyte isotopes for molecular and isobaric interferences (Dulski, 1994, 2001).

During sample analysis, the quality control solution was analyzed approximately every hour. Evaluation of the concentrations measured in the solution throughout the day showed that the instrumental drift was insignificant. The relative standard deviations calculated on the basis of the independent repeated analyses of the quality control solution ranged from 0.5–1.5%RSD at REE concentrations exceeding 1.0 ppm and varied from approximately 1.5–3.0%RSD at concentrations between 0.1 and 1.0 ppm (note that the calculated standard deviations also depend on the isotopic abundance of the isotope used for the ICP-MS determination). In addition to the instrumental drift, the precision and accuracy of the overall analytical procedure were constantly evaluated through repeated independent dissolution and analysis of international reference materials. The precision of the analytical method is in the range of approximately 1–5%RSD for most REEs suggesting that the preparation of the samples (e.g., preparation of homogeneous sample powders, dissolution of the powders, and dilution of the sample solutions) represented a more important source of random errors than instrumental drift. The relative deviations of the analytical results from the recommended values are typically well below ±10% proving that the REE determinations were performed at high accuracy. A detailed discussion of the analytical data obtained on the international reference materials is given in Appendix A.

5. Results

5.1. Sample petrography

Sample MGt-53 represents a white, medium- to coarse-grained, equigranular albite granite. Major rock-forming minerals are quartz, orthoclase, albite, and zinnwaldite. Thin section examination revealed that the sample is intensely altered. Primary plagioclase is pervasively albitized, but sometimes also replaced by white mica (probably $2M_1$ muscovite), illite, and kaolinite. Albitization also affected primary K–feldspar although secondary formation of white mica, illite, and kaolinite at the expense of K–feldspar is more common. Textural evidence suggests that the zinnwaldite represents, at least in part, an alteration product that formed during early greisenization (Li-rich type) whereas the formation of the white mica was apparently related to the late greisenization (Li-poor type). Secondary illite and kaolinite occur in concentrations of ~5 modal %. Fluorite and barite are common secondary accessory phases.

Sample MGr-43 represents a medium-grained, equigranular quartz–zinnwaldite greisen with minor topaz and lepidolite. Only very rare remnants of K–feldspar were observed, whereas plagioclase is completely absent. Li-rich mica flakes are partially replaced by kaolinite. All rock-forming minerals are anhedral in shape. Fluorite, cassiterite, columbite, monazite, and xenotime are common secondary accessory phases. More exotic minerals are unusual members of the philipsbornite–florencite solid solution series (Kempe et al., 1999) and brabandite (Wolf et al., 2002). Accessory zircon shows several distinct styles of secondary alteration (Kempe et al., 1997).

The samples from the Teplice rhyolite contain 20–50 modal % crystals and angular crystal fragments (<8 mm in size) that are set in a fine-grained matrix (grain sizes mainly below 10 μm). The crystals and crystal fragments primarily consist of embayed and partly broken quartz. However, variable amounts of K–feldspar and rare plagioclase (oligoclase to albite) crystals and crystal fragments occur. Fe-rich biotite flakes ranging up to 2 mm in size have been locally observed. An additional common feature is the occurrence of small clusters of closely intergrown chlorite, quartz, Ti-magnetite, fluorite, zircon, and sometimes apatite, rutile, and monazite that are up to several mm in diameter. The matrix of the rhyolite samples is mainly composed of microcrystalline quartz, K–feldspar,

plagioclase (albite), and rare, Fe-rich biotite. Zircon represents the only primary accessory mineral recognized in the matrix. Replacement of the Fe-rich biotite by chlorite and rutile is common. Thin section inspection revealed that the matrix of the rhyolitic samples contains recrystallized welded shards that are commonly deformed, stretched, and compacted at the margins of the crystals and crystal fragments. The observed plastic deformation of the pyroclasts is consistent with the interpretation that the upper part of the Teplice rhyolite represents an ignimbrite.

The samples from the Teplice rhyolite are variably altered. Albitization primarily affected the plagioclase crystals and crystal fragments. Alteration of the matrix plagioclase is less obvious due to their smaller grain sizes. The most prominent alteration of the crystals and crystal fragments occurs in the samples X-2 and L-6a where primary plagioclase is pervasively replaced by chessboard-albite. In the other samples, the degree of albitization is difficult to recognize due to the overprinting effects of later alteration processes. In addition to albitization, greisenization, and argillization affected several samples collected from the Teplice rhyolite. Sample MR-19 contains abundant secondary minerals in the fine-grained matrix including violet fluorite and muscovite. In addition, hematite, zinnwaldite, and kaolinite occur in the matrix of rhyolite collected in the vicinity of the Zinnwald deposit (samples MR-15, MR-19, and MR-14). In these samples, accessory zircon grains exhibit textural and chemical evidence for hydrothermal alteration including replacement structures and anomalously high Fe, Ca, U, and Y contents. The formation of fluorite, associated hematite, and secondary sheet silicates as well as the observed alteration of zircon are tentatively interpreted to be a result of the wall rock greisenization. Late argillization of the plagioclase crystals and crystal fragments was observed in the samples MR-15 and MR-19.

5.2. Major and trace element geochemistry

Whole rock geochemical analysis confirmed the thin section observations that the albite granite MGt-53 is intensely altered. The sample is typified by low Na_2O and high K_2O contents (0.81 wt% Na_2O and 5.65 wt% K_2O) when compared to the less intensely greisenized and argillized albite granite samples from Zinnwald that have average compositions of 3.86 wt% Na_2O and 4.62 wt% K_2O (Seltmann et al., 1998). Complex alteration of the sample MGt-53 resulted in an enrichment of the elements F, Li, Rb, Sn, and Ba. The whole rock geochemical characteristics of the quartz–zinnwaldite greisen MGr-43 are not unlike those of the altered granite (Table 1). However, due to the intense alteration, the greisen sample is typified by even lower Na_2O and CaO contents and shows higher F, Li, Rb, and Sn concentrations.

The geochemical composition of the rhyolite samples also reflects the complex overlap of primary geochemical signatures with chemical changes induced during albitization, greisenization, and argillization. The samples X-2 and L-6a containing abundant secondary chessboard-albite show high overall Na_2O concentrations whereas the least-altered rhyolite L-3 has a somewhat lower Na_2O content. Greisenization and argillization generally caused a decrease in the Na_2O contents. Consequently, the moderately greisenized samples L-4a and MR-14 show elevated Na_2O contents, whereas the intensely altered rhyolite samples MR-15 and MR-19 are typified by very low concentrations of this alkali element. Due to the overprinting effect of the greisenization and argillization, the degree of albitization cannot be readily quantified on the basis of the whole rock geochemical analyses. The degree of greisenization is, however, reflected by an increase in the concentrations of F, Li, Rb, Cs, and Sn, but also resulted in a decrease in the Ba content of the altered whole rock

Table 1
Whole rock geochemical data of the samples from the Zinnwald deposit (major elements and F in wt%, all other data in ppm)

	MGt-53	MGr-43	X-2	L-6a	MR-15	L-4a	MR-19	MR-14	L-3
SiO_2	73.00	79.41	73.81	75.18	76.25	77.05	80.31	75.25	75.35
TiO_2	0.01	0.01	0.05	0.05	0.12	0.12	0.14	0.16	0.11
Al_2O_3	15.19	8.61	12.49	12.86	12.13	12.4	9.64	12.73	12.57
Fe_2O_3	0.98	3.18	1.02	1.01	1.94	1.59	2.04	1.56	1.84
MnO	0.09	0.41	0.03	0.03	0.04	<0.02	0.17	0.08	<0.02
MgO	0.17	<0.10	<0.10	<0.10	0.15	0.12	0.13	0.12	0.17
CaO	0.43	0.23	0.53	0.79	0.70	0.50	0.77	0.77	0.10
Na_2O	0.81	0.05	3.71	3.73	0.38	2.97	0.31	1.66	2.01
K_2O	5.65	4.15	4.33	4.53	6.41	5.24	3.99	6.01	6.23
P_2O_5	0.02	0.01	0.02	0.03	0.01	0.02	0.02	0.03	0.01
SO_3	0.02	<0.01	<0.01	<0.01	<0.01	<0.01	<0.01	<0.01	<0.01
LOI	3.09	1.51	0.86	0.89	1.88	0.70	1.86	1.52	0.97
F	0.58	3.73	0.38	0.52	0.82	0.20	2.49	0.75	0.11
Li	1150	4605	nd	nd	451	66	1365	115	20
Cs	26	136	24	25	48	10	47	33	<8
Rb	2441	3604	901	898	1273	387	1680	571	361
Sn	166	758	38	35	20	15	184	66	<10
Ba	714	131	8.4	13	216	117	134	229	224

Notes: All iron is given as Fe_2O_3. LOI, loss on ignition. nd, not determined.

samples. Argillization is typified by the addition of F and Ba (Table 1).

5.3. Rare earth element data

To constrain the sample and element specific random errors of the ICP-MS determinations, all samples from the Zinnwald deposit were repeatedly dissolved and analyzed. Appendix B gives the results of the 5–10 independent sample preparations and analyses along with the calculated averages, standard deviations, and relative standard deviations. A summary of the REE data is given in Table 2.

Fig. 2 shows the normalized REE patterns of the altered granite sample MGt-53 and the greisen MGr-43. Both endocontact samples exhibit kinked REE patterns, the normalized REE concentrations decrease from La to Gd and increase from Gd to Lu. The kinks in the REE patterns are camouflaged by prominent convex tetrads and pronounced negative Eu anomalies (Eu/Eu* ratios of 0.05 and 0.01). Visual inspection suggests that the first tetrad is more prominent than the third and fourth curved segments. The second tetrad is comparably difficult to recognize due to the anomalous behavior of Eu and the fact that Pm does not occur in nature.

The two intensely albitized rhyolite samples X-2 and L-6a exhibit relatively flat REE patterns (Fig. 3). The normalized REE concentrations decrease slightly from La to Gd and increase from Gd onwards. Both patterns show noticeable tetrads and prominent negative Eu anomalies with an Eu/Eu* ratio of 0.01. In both rhyolite samples, only the first and third tetrads are prominent and readily recognizable as curved segments.

All other samples from the Teplice rhyolite are typified by pronounced enrichments of the light REEs (Figs. 4 and 5). The normalized REE patterns of the samples MR-15 and MR-19 exhibit steep slopes from La to Gd, but are almost horizontal between Gd and Lu (Table 2). Both samples exhibit prominent negative Eu anomalies (Eu/Eu* ratios of 0.06 and 0.12). In contrast to these two rhyolite samples, the normalized REE concentrations of the samples L-4a, MR-14, and L-3 decrease continuously from La to Lu, but also show prominent negative Eu anomalies (Eu/Eu* values of 0.07–0.14). Although the first, third, and fourth tetrads in sample MR-15 are small in size, curvature of these segments can be readily recognized. In contrast, the rhyolite L-4a only shows notable curvature of the first and third tetrads. The existence of tetrads in the samples MR-19, MR-14, and L-3 is ambiguous (Fig. 5).

Quantification of the tetrad sizes was carried out in analogy to the method proposed by Monecke et al. (2002). These authors suggested that the tetrad sizes in logarithmically scaled normalized REE patterns, denoted as T_i, where $i = 1...4$ is the number of the respective tetrad, are best represented by the deviations of the two central elements within each tetrad from a straight line connecting the contents of the first and the last element of the tetrad. The value of T_i is zero if all four elements of the tetrad i plot on a straight line, whereas $T_i > 0$ if the tetrad is either convex or concave. In the present case, the arithmetic mean values calculated on the basis of the repeated independent sample preparations and analyses (Appendix B) have been used to quantify the tetrad sizes (Table 3).

Monecke et al. (2002) proposed that a given tetrad i is only significant if the calculated T_i value exceeds a certain level of significance calculated from estimated analytical errors. In contrast to the study of Monecke et al. (2002) that was based only on a single determination of the REE concentrations in each sample, the element and sample specific standard deviations of the REE measurements have been constrained in the present case. Thus, it is now possible

Table 2
Rare earth element concentrations of the samples from the Zinnwald deposit (all data in ppm)

	MGt-53	MGr-43	X-2	L-6a	MR-15	L-4a	MR-19	MR-14	L-3
La	16.8	11.9	21.1	22.0	54.4	64.5	51.5	67.7	37.6
Ce	49.6	35.9	51.3	55.6	114	130	103	137	78.7
Pr	5.72	4.09	7.01	7.53	13.3	15.1	12.4	15.4	10.6
Nd	15.1	10.8	27.0	29.6	46.5	53.0	43.7	53.5	38.7
Sm	4.49	3.11	9.21	10.5	10.9	11.5	9.41	10.9	8.51
Eu	0.057	0.012	0.023	0.024	0.220	0.262	0.344	0.454	0.270
Gd	2.81	2.20	10.6	12.6	10.3	10.6	8.22	9.48	7.47
Tb	0.747	0.614	2.27	2.74	1.84	1.83	1.40	1.55	1.21
Dy	5.68	4.72	16.4	19.5	11.6	11.4	8.67	9.28	7.29
Ho	1.18	0.965	3.62	4.20	2.32	2.30	1.71	1.81	1.42
Er	4.56	3.73	12.0	13.3	6.94	6.59	5.13	5.25	4.05
Tm	0.983	0.825	2.00	2.13	1.06	0.955	0.799	0.728	0.584
Yb	8.97	7.66	14.0	14.7	7.17	5.94	5.58	4.69	3.82
Lu	1.35	1.14	2.07	2.13	1.03	0.859	0.806	0.672	0.554
La_n/Gd_n	5.01	4.54	1.67	1.46	4.42	5.12	5.25	5.98	4.22
Gd_n/Lu_n	0.26	0.24	0.63	0.73	1.24	1.52	1.26	1.74	1.67
Eu/Eu*	0.05	0.01	0.01	0.01	0.06	0.07	0.12	0.14	0.10

Note: The data represent the arithmetic mean values derived from 5–10 repeated independent sample preparations and measurements (Appendix B). The normalization is based on the chondrite data given by Anders and Grevesse (1989). The Eu anomaly is defined as $Eu/Eu^* = Eu_n/\sqrt{Sm_n \times Gd_n}$.

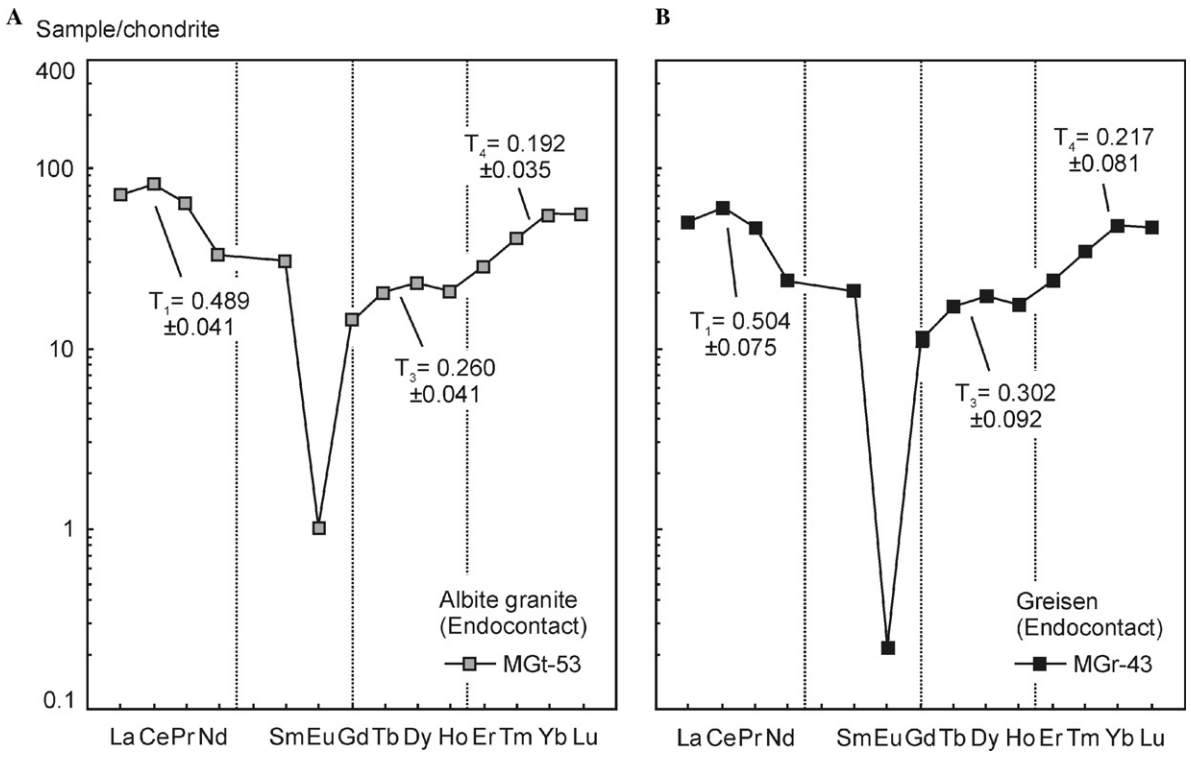

Fig. 2. Normalized REE patterns of the altered granite sample MGt-53 and the greisen MGr-43 from the Zinnwald deposit. The plotted REE concentrations represent the arithmetic mean values derived from repeated independent preparations and measurements of both samples. The normalization is based on the chondrite data given by Anders and Grevesse (1989). See text for details on the quantification of the tetrad sizes.

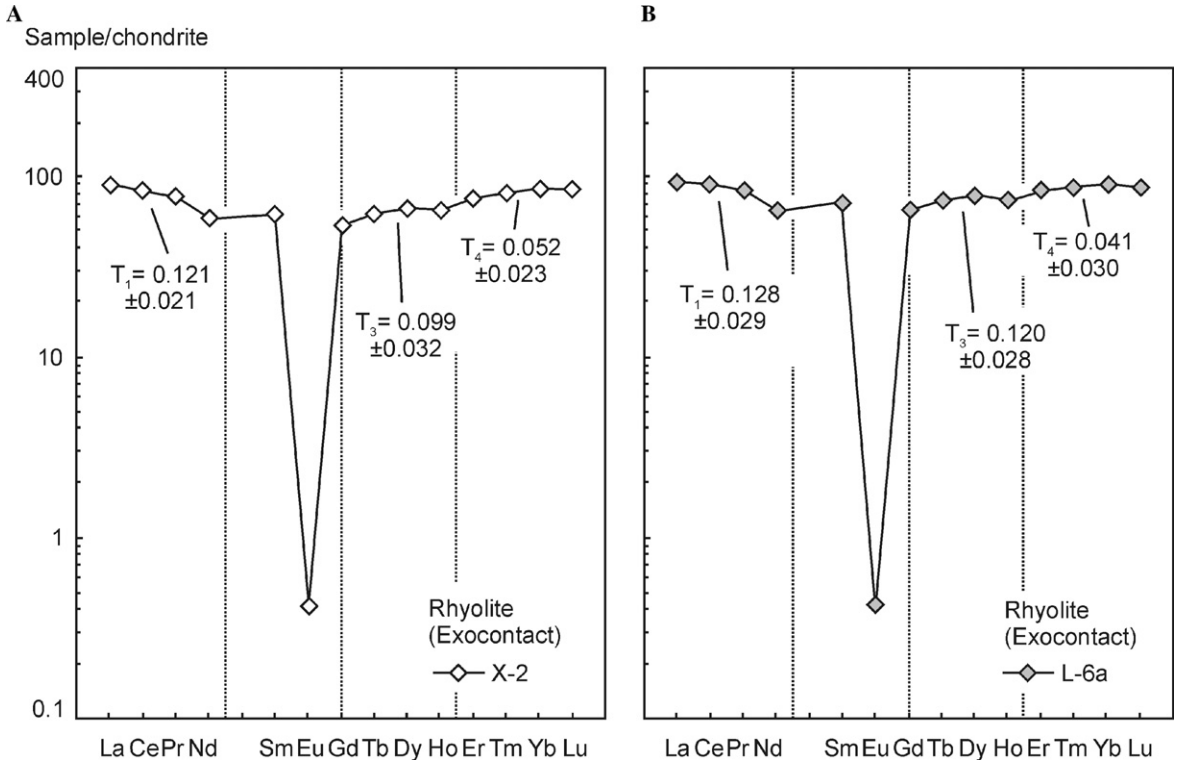

Fig. 3. Normalized REE patterns of the albitized rhyolite samples X-2 and L-6a from the Zinnwald deposit. The plotted REE concentrations represent the arithmetic mean values derived from repeated independent preparations and measurements of both samples. The normalization is based on the chondrite data given by Anders and Grevesse (1989). See text for details on the quantification of the tetrad sizes.

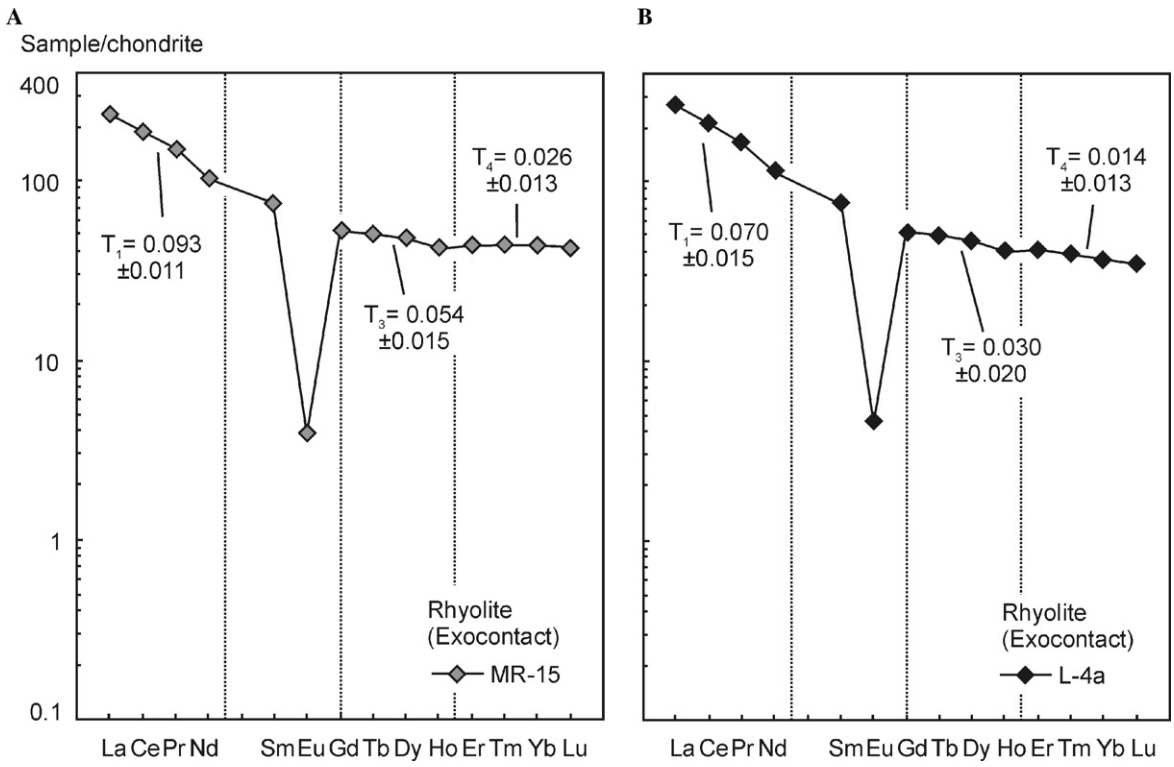

Fig. 4. Normalized REE patterns of the altered rhyolite samples MR-15 and L-4a from the Zinnwald deposit. The plotted REE concentrations represent the arithmetic mean values derived from repeated independent preparations and measurements of both samples. The normalization is based on the chondrite data given by Anders and Grevesse (1989). See text for details on the quantification of the tetrad sizes.

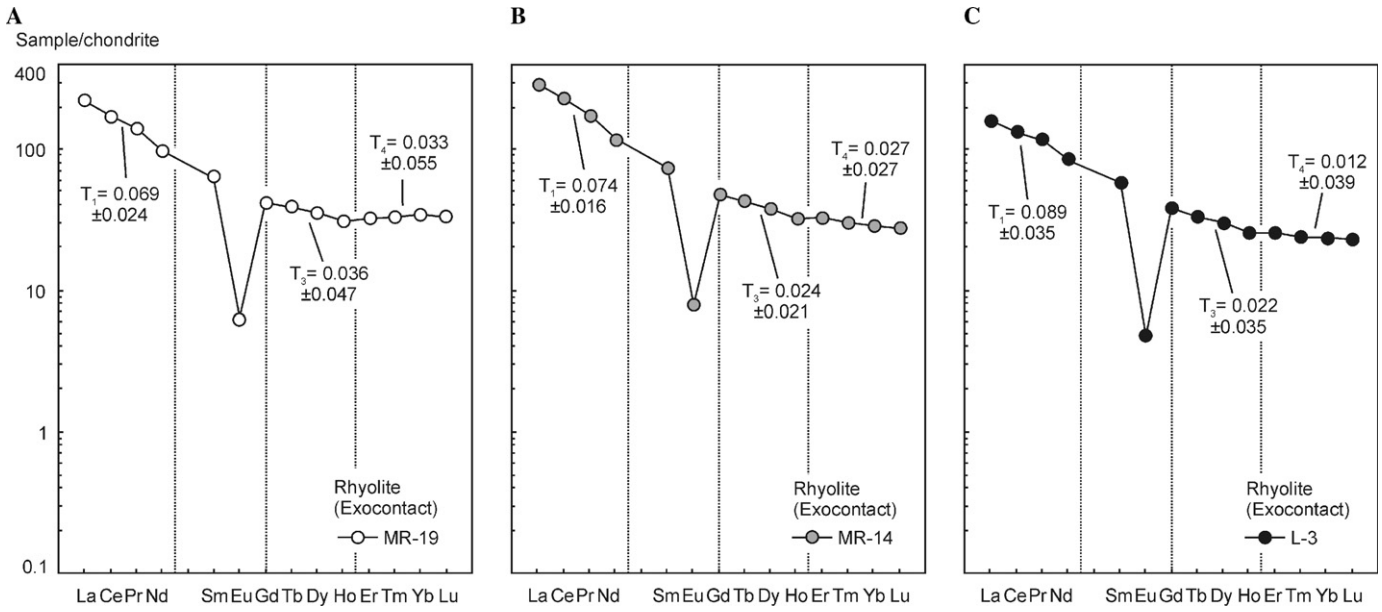

Fig. 5. Normalized REE patterns of the altered rhyolite samples MR-19, MR-14, and L-3 from the Zinnwald deposit. The plotted REE concentrations represent the arithmetic mean values derived from repeated independent preparations and measurements of both samples. The normalization is based on the chondrite data given by Anders and Grevesse (1989). See text for details on the quantification of the tetrad sizes.

to judge the significance of a given tetrad i by calculating the standard deviation of the size of the respective tetrad from the element and sample specific standard deviations applying the error propagation law of Gauss. The standard deviations of the T_i values are then given by

$$\sigma_{T_i}^2 = \sum_{e=1}^{4} \left[\left(\frac{\partial T_i}{\partial x_e} \right) \sigma_{x_e} \right]^2 \quad (1)$$

with e denoting the four elements forming the tetrad i and the σ_{x_e} being the standard deviations of the concentrations

of the four elements. The values of the derivatives ($\partial T_i/\partial x_e$) are calculated at the mean concentrations $\bar{x}_e$. This approach is of advantage because the standard deviations of the tetrad sizes could be used, e.g., in the calculation of confidence intervals or the construction of error bars in plots correlating the sizes of tetrads with other geochemical parameters. The derived standard deviations and 99% confidence intervals of the T_i values are listed in Table 3.

Based on a visual examination of the normalized REE patterns and the calculated confidence intervals, it is possible to evaluate the significance of the tetrads. Inspection of Table 3 shows that all three quantifiable tetrads in the REE patterns of the albite granite and greisen samples are significant from the analytical point of view. In both cases, the first tetrad is larger in size than the third and fourth curved segments. In the exocontact samples, only the intensely albitized rhyolite samples X-2 and L-6a show three significant tetrads at the 99% confidence level. The first curved segments always represent the largest tetrads. The sample MR-15 is also typified by three significant tetrads, but the fourth tetrad is only significant at the 99% confidence level because the sample preparation and analysis was repeated ten times (Table 3). The rhyolite L-4a is typified by significant first and third tetrads, the fourth tetrad is, however, not unequivocally recognizable at this confidence level. Careful error evaluation as performed in the present study further established that only the first tetrad is significant in the samples MR-19 and MR-14. The rhyolite L-3 lacks significant tetrads although the deviation of Ce from a straight line connecting La and Nd in the normalized REE plot (Fig. 5) is significant from the analytical point of view.

Table 3
Sizes and confidence intervals of tetrads in the rare earth element patterns. The significance of the tetrads was judged on the basis of the confidence intervals and visual inspection of the normalized rare earth element plots

Sample	Tetrad	T	SD	$\pm\Delta T$	Significance
MGt-53	1	0.489	0.020	0.041	Yes
	3	0.260	0.020	0.041	Yes
	4	0.192	0.017	0.035	Yes
MGr-43	1	0.504	0.036	0.075	Yes
	3	0.302	0.045	0.092	Yes
	4	0.217	0.039	0.081	Yes
X-2	1	0.121	0.010	0.021	Yes
	3	0.099	0.015	0.032	Yes
	4	0.052	0.011	0.023	Yes
L-6a	1	0.128	0.014	0.029	Yes
	3	0.120	0.014	0.028	Yes
	4	0.041	0.015	0.030	Yes
MR-15	1	0.093	0.011	0.011	Yes
	3	0.054	0.015	0.015	Yes
	4	0.026	0.013	0.013	Yes
L-4a	1	0.070	0.007	0.015	Yes
	3	0.030	0.010	0.020	Yes
	4	0.014	0.006	0.013	No
MR-19	1	0.069	0.012	0.024	Yes
	3	0.036	0.023	0.047	No
	4	0.033	0.027	0.055	No
MR-14	1	0.074	0.008	0.016	Yes
	3	0.024	0.010	0.021	No
	4	0.027	0.013	0.027	No
L-3	1	0.089	0.017	0.035	No
	3	0.022	0.017	0.035	No
	4	0.012	0.019	0.039	No

Notes: The data are calculated on the basis of the 5–10 repeated independent sample preparations and measurements (Appendix B). SD, standard deviation; $\pm\Delta T = 99\%$ confidence interval (calculated as $4.605\mathrm{SD}\sqrt{n}$ for $n = 5$ and $3.250\mathrm{SD}\sqrt{n}$ for $n = 10$).

6. Discussion

6.1. Analytical significance of subtle tetrads

McLennan (1994) showed that the recognition of subtle tetrads in normalized REE patterns requires the use of a highly precise and accurate analytical procedure that allows the determination of complete REE patterns. Error calculations forming part of previous investigations (Monecke et al., 2002, 2003) illustrated that a precision of 5 to 10 %RSD, characteristic for ICP-MS investigations on whole rock samples containing abundant refractory phases such as zircon, is indeed insufficient to warrant geochemical interpretation of subtle tetrads in rocks collected from evolved granitic systems.

In contrast to earlier studies that used estimated random errors (Monecke et al., 2002, 2003; Takahashi et al., 2003), the present study aimed to directly constrain the element and sample specific random errors of the REE determinations through repeated independent sample preparation and analysis. Optimization of the analytical procedure and in particular, the method of sample dissolution, showed that ICP-MS measurements on whole rock samples from evolved granitic systems are routinely possible at a precision ranging from approximately 1–3%RSD for most REEs.

Rigorous statistical treatment at the 99% confidence interval demonstrates that all quantifiable curved segments in the REE patterns of the endocontact samples from the Zinnwald deposit cannot be explained by the random errors of the REE determination (Table 3). Comparison of the results of the present study to the findings of Monecke et al. (2002) shows that repeated sample preparation and analysis allowed the recognition of the subtle fourth tetrads in the endocontact samples that could not be unequivocally identified on the basis of a single ICP-MS measurement. In contrast to the endocontact samples, the rhyolitic wall rocks do not always exhibit three analytically significant tetrads. The petrographic evidence suggests that the number of significant tetrads correlates with the style and intensity of hydrothermal alteration. The earlier study by Monecke et al. (2002) failed to recognize this relationship because single ICP-MS measurement of the whole rocks did not allow the identification of subtle tetrads. It is, therefore, proposed here that repeated sample preparation and analysis should be routinely performed if subtle tetrads are studied.

The present investigation shows that five independent preparations and analyses are typically sufficient to prove the existence of subtle tetrads having T_i values of approximately 0.100–0.200. However, a further increase in the number of analyses may be required to test for even smaller tetrads. For instance, ten independent sample preparations and analyses were required to identify the very subtle fourth tetrad in the REE pattern of the rhyolite sample MR-15 at the 99% confidence level. The example highlights the fact that the chosen analytical strategy is a critical factor in the decision whether geochemical relevance should be attributed to subtle curved segments in normalized REE patterns.

In addition to the discussion of the random errors of the ICP-MS investigations, it is important to evaluate the accuracy of the analytical method to ensure that subtle tetrads are not introduced by systematic errors. In the present case, systematic errors of the ICP-MS measurements were ruled out as an explanation for the observed tetrads because the measurement of international reference materials yielded results that are in good agreement with the recommended values (Appendix A). In addition, no significant tetrads were observed in the REE patterns of the reference materials. Assuming that the specific chemistry of the investigated samples did not induce any systematic bias, this indicates that tetrads in the whole rock samples from Zinnwald cannot be accounted for by analytical difficulties. The samples and reference materials were analyzed simultaneously under identical analytical conditions. Although there is no evidence supporting the assumption that artificial tetrads can be introduced at all during rock dissolution in PTFE vessels and subsequent ICP-MS analysis as carried out in the present study, it is important to note that the situation may be different if the REEs have to be enriched from highly dilute solutions such as water samples, e.g., by the ferric hydroxide co-precipitation method (Wood, 2003).

Because random and systematic errors of the REE determinations cannot explain most of the tetrads observable in the normalized REE patterns of endo- and exocontact samples from the granite-hosted Zinnwald deposit, Germany, the question arises which geochemical process is responsible for the development of the curved convex segments.

6.2. Genetic significance of subtle tetrads

Following the arguments of Bau (1997) and Irber (1999), it is unlikely that the three quantifiable tetrads in the REE patterns of the endocontact samples from the Zinnwald deposit represent a result of fractional crystallization of accessory phases, especially since garnet or primary xenotime have not been observed in granite and greisen from this locality.

ICP-MS analysis of albite granite and greisen samples revealed that the tetrads in the REE patterns of both rock types have similar sizes (Fig. 2), a fact already noted by Sala (1999) and Monecke et al. (2002). This observation suggests that sub-solidus greisenization was not responsible for the development of the convex tetrads in the endocontact samples. However, Sala (1999) showed that the albite granite has, in general, slightly higher overall lanthanide concentrations suggesting that the greisenization resulted in a remobilization of the REEs. This suggestion is consistent with the occurrence of abundant secondary REE-bearing phosphates, arsenates, and sulfates in the greisen (Kempe et al., 1999; Wolf et al., 2002).

In addition to greisenization, late stage argillization was found to be widespread in the endocontact of the Zinnwald granite massif. Low-temperature argillization primarily affected the albite granite, but is not well developed in the greisen because feldspar readily accessible to argillization does not represent a major component of this rock type. Furthermore, because there is no correlation between the tetrad sizes and the degree of argillization (Sala, 1999), the development of the convex tetrads in endocontact samples can also not be linked to this style of hydrothermal alteration.

Combined with the geological relationships, the geochemical evidence implies that the convex segments in the REE patterns of the endocontact samples formed prior to the greisenization and the late stage argillization (surface weathering did not affect the underground samples). Therefore, it has to be concluded that the development of the tetrads in the endocontact samples was linked to either a hitherto unrecognized process occurring during the magmatic evolution of the granitic melt or, alternatively, to the albitization of the granite that predates greisenization and ore deposition.

In analogy to the samples from the endocontact, it is unlikely that fractional crystallization caused the tetrads in the rhyolite samples of the exocontact. In particular, the observed variations in the tetrad sizes cannot be readily accounted for by models linking the tetrad effect to the evolution of the rhyolitic magma at depth prior to its eruption as an ignimbrite. Correlation of the tetrad sizes with the style and intensity of hydrothermal alteration suggests that the tetrads represent a result of the interaction of the Teplice rhyolite with hydrothermal fluids related to the granite intrusion. However, it is important to note that least-altered rhyolite samples show a subtle curvature of the first tetrad. It is proposed here that at least two tetrads in whole rock REE patterns have to be analytically significant to postulate the occurrence of the tetrad effect.

Based on the results of the whole rock geochemical analysis, the extent of greisenization and argillization of the rhyolite samples can be readily estimated and compared to the calculated sizes of the tetrads. Although pronounced tetrads have been observed in some altered rhyolite samples, there is no correlation between the tetrad sizes and the whole rock F, Li, Rb, Cs, and Sn concentrations (Tables 1 and 3). In particular, it is important to note that the rhyolite MR-19, the sample that has been affected by most intense greisenization and argillization, shows only one analytically significant tetrad. Greisenization and the

spatially more restricted argillization in the exocontact are, therefore, not linked to the formation of the curved segments in the REE patterns of the wall rocks.

In contrast to greisenization and argillization, the degree of albitization of the rhyolite samples is difficult to estimate on the basis of the whole rock geochemical data. The most prominent chemical effect related to formation of secondary albite is an increase in the whole rock Na_2O content. However, subsequent greisenization resulted in decreasing Na_2O concentrations. Thus, thin section inspection provides the only reliable information constraining the degree of albitization of the rhyolitic wall rocks. Intense albitization of plagioclase crystals and crystal fragments was observed in the samples X-2 and L-6a. Both samples are typified by flat REE patterns showing three significant tetrads at the 99% confidence level. The rhyolite MR-15, a third sample with three significant tetrads at this level of confidence, was affected by intense greisenization and argillization overprinting earlier albitization. Due to the pervasive replacement of the primary plagioclase crystals and crystal fragments, the degree of albitization could not be estimated by optical microscopy. No evidence for albitization could be found in the samples L-4a, MR-19, MR-14, and L-3 that are only typified by one or two significant tetrads. Based on these observations, it is proposed that the tetrads in the exocontact samples are most probably linked to the albitization of the rhyolitic wall rocks.

The findings of the present study demonstrate that the tetrads in the REE patterns of endocontact rocks from the Zinnwald Sn–W deposit, Germany, formed either in response to a hitherto unconstrained process early in the evolution of the magmatic–hydrothermal system or during the hydrothermal albitization of the granite massif at sub-solidus conditions. In contrast, the tetrads in the REE patterns of the wall rocks were clearly introduced during the interaction of the rhyolite with the hydrothermal fluids. Formation of the tetrads predated the greisenization of the granite and the surrounding wall rocks and the formation of the tin ores.

Based on an extensive geochemical survey on fluorite from Sn deposits (Kempe and Goldstein, 1997) and the results of previous experimental investigations (Peppard et al., 1969; Veksler et al., 2005), it is assumed here that the occurrence of the tetrad effect during the evolution of the magmatic–hydrothermal system at Zinnwald is linked to processes of phase separation. At present, two possible scenarios of tetrad formation are consistent with the geological and geochemical evidence.

As a first scenario it may be assumed that the evolution of the magmatic–hydrothermal system at Zinnwald was accompanied by the unmixing of an originally homogeneous melt at super-liquidus conditions. As a result, convex tetrads were formed in the silicate melt that intruded in the subvolcanic environment, whereas the complimentary REE pattern must have been removed from the subvolcanic environment into an immiscible, currently unrecognized, phase. In this case, the granite may already have possessed convex tetrads prior to hydrothermal alteration at sub-solidus conditions. The hydrothermal fluids involved in the early albitization of the granite may then have inherited the unusual geochemical signature from the endocontact rocks. Outward migration of the hydrothermal fluids into the surrounding wall rocks resulted in the albitization of the Teplice rhyolite. The subtle tetrads in the REE patterns of the wall rock are consequently a direct result of the hydrothermal overprint by fluids already showing convex tetrads following their interaction with the granite. Support for this model comes from a melt inclusion study that suggests that the evolution of the magmatic–hydrothermal system at Zinnwald was indeed accompanied by the unmixing of an originally homogeneous melt into two phases at super-liquidus conditions (Thomas et al., 2005). However, it is important to note that intense secondary alteration is widespread in the upper portion of the granite massif. Currently, it cannot be ruled out that melt inclusions hosted by primary minerals such as quartz have not been compositionally modified during secondary alteration.

Alternatively, it is possible that the granite at Zinnwald was not typified by tetrads prior to hydrothermal alteration at sub-solidus conditions. In this case, phase separation in the hydrothermal environment may have generated an aqueous fluid showing convex tetrads, and a second, currently not recognized, phase with concave tetrads. Interaction of the granite and rhyolite with the aqueous fluid showing convex tetrads resulted in the albitization of the endo- and exocontact rocks and the development of M-shaped whole rock REE patterns. In this scenario, the observed differences in the tetrad sizes of the endo- and exocontact rocks are probably best explained by a distinct change in the rate of REE fractionation at the contact between the granite and the wall rocks or a pronounced decrease in the intensity of fluid–rock interaction across the contact. Although it is currently unknown whether albitization of the granite and the surrounding rhyolite at Zinnwald was accompanied by unmixing of an originally homogeneous hydrothermal fluid, fluid inclusion investigations suggest that phase separation occurred during the evolution of the hydrothermal system (Ďurišová et al., 1979; Heinrich et al., 1999). It remains, however, unclear why mineral and rock samples exhibiting complementary W-shaped REE patterns have not yet been found anywhere in the Zinnwald magmatic–hydrothermal system.

The geochemical processes involved in the development of convex tetrads are complex. Both scenarios described above should be considered as 'end-member' models. It cannot be ruled out that a combination of both scenarios involving repeated unmixing of melts and/or hydrothermal fluids took place during the evolution of the evolved tin-bearing magmatic–hydrothermal system at Zinnwald. Comparison of the analytical results of the present contribution to granite data from other tin deposits in the Erzgebirge (Irber, 1999) shows that the three quantifiable tetrads in the whole rock REE patterns have variable relative sizes where either the first or the third tetrad is dominant. Thus,

more than one process may be required to explain both the occurrence of tetrads in the evolved granitic systems as well as the variations in the relative sizes of the tetrads between individual deposits.

7. Conclusions

The present study demonstrates that the occurrence of subtle convex (M-shaped) tetrads in normalized REE patterns of whole rock samples from the granite-hosted Zinnwald Sn–W deposit, Germany, cannot be accounted for by analytical uncertainties. Based on repeated independent preparations and analyses of samples and international reference materials, the element and sample specific random and systematic errors of the ICP-MS measurements have been determined. Error evaluation revealed that endocontact granite and greisen samples are typified by significant convex tetrads whereas the tetrad sizes of exocontact rhyolite samples are frequently close to, or below, the limit of analytical significance. The observed tetrads cannot be accounted for by systematic errors because simultaneous analysis of international reference materials demonstrated that the REE determinations were performed at high accuracy. Despite increased analytical costs, it is proposed that the developed analytical method should be used routinely in the study of whole rock samples exhibiting subtle tetrads.

Critical discussion of the data demonstrates that the presence of a single analytically significant curved segment in the REE patterns of whole rock samples from evolved granitic systems is insufficient to rule out that the unusual behavior of the REEs is not related to fractional crystallization. It is proposed that at least two curved segments have to be confidently identified to allow the conclusion that the fractionation of the REEs during the evolution of a given magmatic–hydrothermal system is related to the lanthanide tetrad effect.

Based on the geological, petrographic, and geochemical evidence, some preliminary conclusions can be drawn on the occurrence of the lanthanide tetrad effect during the evolution of the magmatic–hydrothermal system at Zinnwald. In the case of the endocontact rocks, the convex tetrads must have developed prior to the hydrothermal greisenization and the main stage ore formation, presumably in response to phase separation at super-liquidus conditions or unmixing of an originally homogeneous hydrothermal fluid during the early albitization of the granite massif. In contrast to endocontact samples, the convex tetrads in the normalized REE patterns of rhyolitic wall rocks clearly formed during sub-solidus alteration, the size of the tetrads apparently correlates with the intensity of albitization. The hydrothermal fluids involved in the albitization of the rhyolitic wall rocks acquired their unusual REE signatures during sub-solidus interaction with the endocontact rocks or as a result of processes of phase separation in the hydrothermal environment. The convex tetrads in the endo- and exocontact samples from the Zinnwald deposit were not introduced during late stage argillitization or surface weathering.

Further detailed investigations on rock and mineral samples are required to determine whether the lanthanide tetrad effect in evolved granitic systems associated with rare metal deposits is confined to the magmatic or hydrothermal environment. Significant advances in the field are predicted once host minerals of melt or fluid inclusions are found that show REE patterns with concave (W-shaped) tetrads.

Acknowledgments

We thank G. Matheis and L. Domin for conducting the XRF analyses. J. Hutschenreuter, M. Sala, and T. Schlothauer helped us during field work at Zinnwald. We acknowledge valuable comments on the geology of the Zinnwald deposit by R. Seltmann and D. Wolf. The manuscript also benefited from fruitful discussions with J. Monecke. Reviews by two anonymous reviewers and comments by R.H. Byrne helped us to improve an earlier version of the manuscript. Initial studies on the significance of the tetrad effect in the samples investigated were carried out by T.M. while in receipt of a scholarship by the German National Merit Foundation. Subsequent funding to T.M. was provided by the German Research Foundation.

Associate editor: Robert H. Byrne

Appendix A. Repeated independent preparation and analysis ofreference materials

The quality of the applied analytical procedure was evaluated on the basis of repeated independent preparations and analyses of a wide range of international reference materials that bracket the composition of the samples from the Zinnwald deposit. As an example, the REE concentrations of five independent preparations and analyses of the reference materials BVHO-1 (basalt from the Kilauea caldera, Kilauea volcano, Hawaii) and G-2 (granite from Sullivan quarry, Bradford, Rhode Island, USA) are given in Tables A1 and A2 along with the respective arithmetic mean values, standard deviations, and relative standard deviations.

The results of the repeated analyses of the two reference materials demonstrate that the precision of the analytical method was below 5%RSD for most elements. The precision of the REE determinations is visualized in Fig. A1 by calculating the ratios between the analyte content determined for each run and the mean value of the five independent sample preparations and measurements. Inspection of the plots illustrates that large spreads in the REE determination can be observed only for certain analytes, in most cases these analytes are typified by low concentrations. The observed random errors are interpreted to have been largely introduced during the preparation of the samples (e.g., preparation of homogeneous sample powders, disso-

Table A1
Rare earth element concentrations in the reference material BHVO-1 (all data in ppm)

	1	2	3	4	5	Mean	SD	%RSD
La	15.6	15.3	15.5	15.2	15.6	15.4	0.2	1.2
Ce	38.2	37.9	37.8	37.3	38.5	37.9	0.5	1.2
Pr	5.56	5.58	5.52	5.50	5.69	5.57	0.07	1.3
Nd	24.1	24.3	24.3	23.8	24.8	24.3	0.4	1.5
Sm	6.03	5.96	6.02	5.82	6.05	5.98	0.09	1.6
Eu	2.10	2.15	2.06	2.05	2.09	2.09	0.04	1.9
Gd	6.57	6.52	6.52	6.31	6.69	6.52	0.14	2.1
Tb	0.935	0.951	0.923	0.910	0.960	0.936	0.020	2.2
Dy	5.38	5.32	5.25	5.21	5.53	5.34	0.13	2.4
Ho	1.00	0.961	0.980	0.939	0.991	0.974	0.024	2.5
Er	2.56	2.57	2.50	2.49	2.61	2.55	0.05	2.0
Tm	0.330	0.334	0.334	0.327	0.334	0.332	0.003	1.0
Yb	1.94	2.19	2.17	2.15	2.02	2.09	0.11	5.2
Lu	0.283	0.283	0.271	0.275	0.290	0.280	0.007	2.7

Notes: SD, standard deviation; %RSD, relative standard deviation in %.

lution of the powders, and dilution of the sample solutions) although instrumental drift clearly contributed to the spread in the analytical results. In general, the REEs were less precisely determined in the granitic reference material G-2 than in the basalt BVHO-1. This observation is most readily explained by the presence of refractory REE-bearing minerals such as zircon hampering quantitative sample dissolution.

The accuracy of the REE determinations can be judged by comparing the mean values determined for the reference materials with the reference values given by Govindaraju (1994) and data obtained by other workers (Table A3). Plots displaying the ratios between the REE concentrations determined by other workers and those of the present contribution are given in Fig. A2. The plots illustrate that the agreement between the different data sets is very good for the basalt reference material BHVO-1 (<5% deviation for most elements) whereas the analyses of the granite G-2 are typified by larger discrepancies (<10% deviation for most elements), particularly for the HREEs. In the case

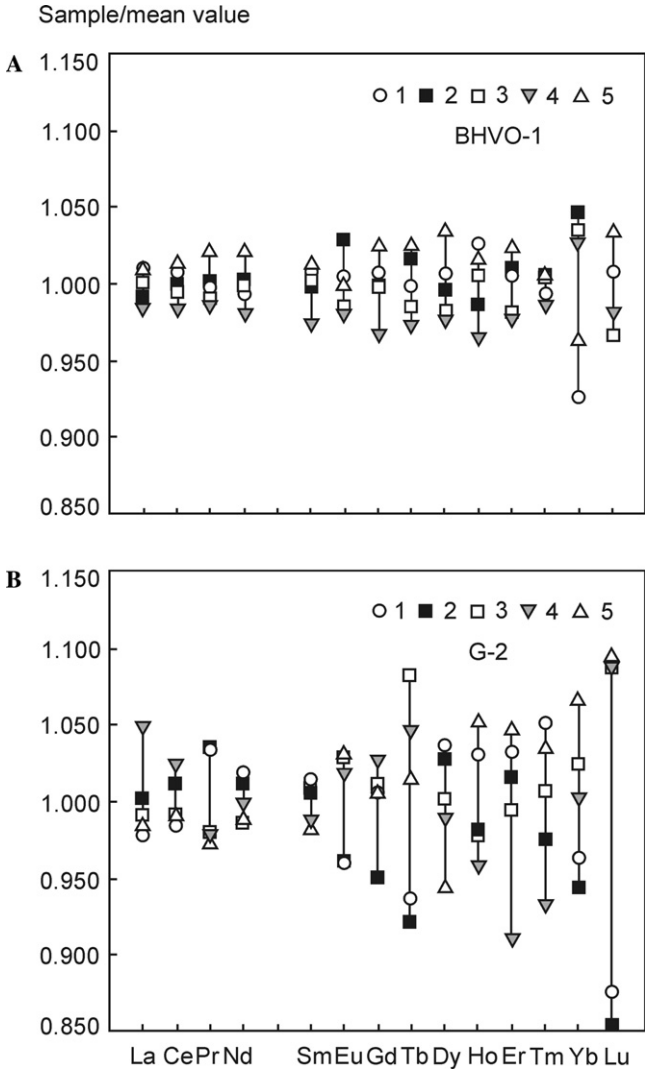

Fig. A1. Ratios between the REE contents in the international reference materials BHVO-1 and G-2 determined for each run and the mean value derived from repeated independent preparations and measurements.

Table A2
Rare earth element concentrations in the reference material G-2 (all data in ppm)

	1	2	3	4	5	Mean	SD	%RSD
La	85.2	87.3	86.3	91.3	85.7	87.2	2.4	2.8
Ce	156	160	157	162	157	158	3	1.6
Pr	16.9	16.9	16.0	16.0	15.9	16.3	0.5	3.1
Nd	52.8	52.4	51.2	51.7	51.2	51.9	0.7	1.4
Sm	6.98	6.92	6.96	6.79	6.76	6.88	0.10	1.5
Eu	1.38	1.38	1.48	1.46	1.48	1.44	0.05	3.6
Gd	4.23	3.99	4.25	4.31	4.23	4.20	0.12	2.9
Tb	0.469	0.461	0.542	0.523	0.508	0.501	0.035	6.9
Dy	2.15	2.13	2.08	2.05	1.96	2.07	0.08	3.6
Ho	0.364	0.347	0.346	0.338	0.372	0.353	0.014	4.0
Er	0.915	0.900	0.881	0.806	0.928	0.886	0.048	5.4
Tm	0.123	0.114	0.118	0.109	0.121	0.117	0.006	4.8
Yb	0.707	0.693	0.753	0.735	0.784	0.734	0.036	4.9
Lu	0.108	0.105	0.134	0.134	0.135	0.123	0.015	12.4

Notes: SD, standard deviation; %RSD, relative standard deviation in %.

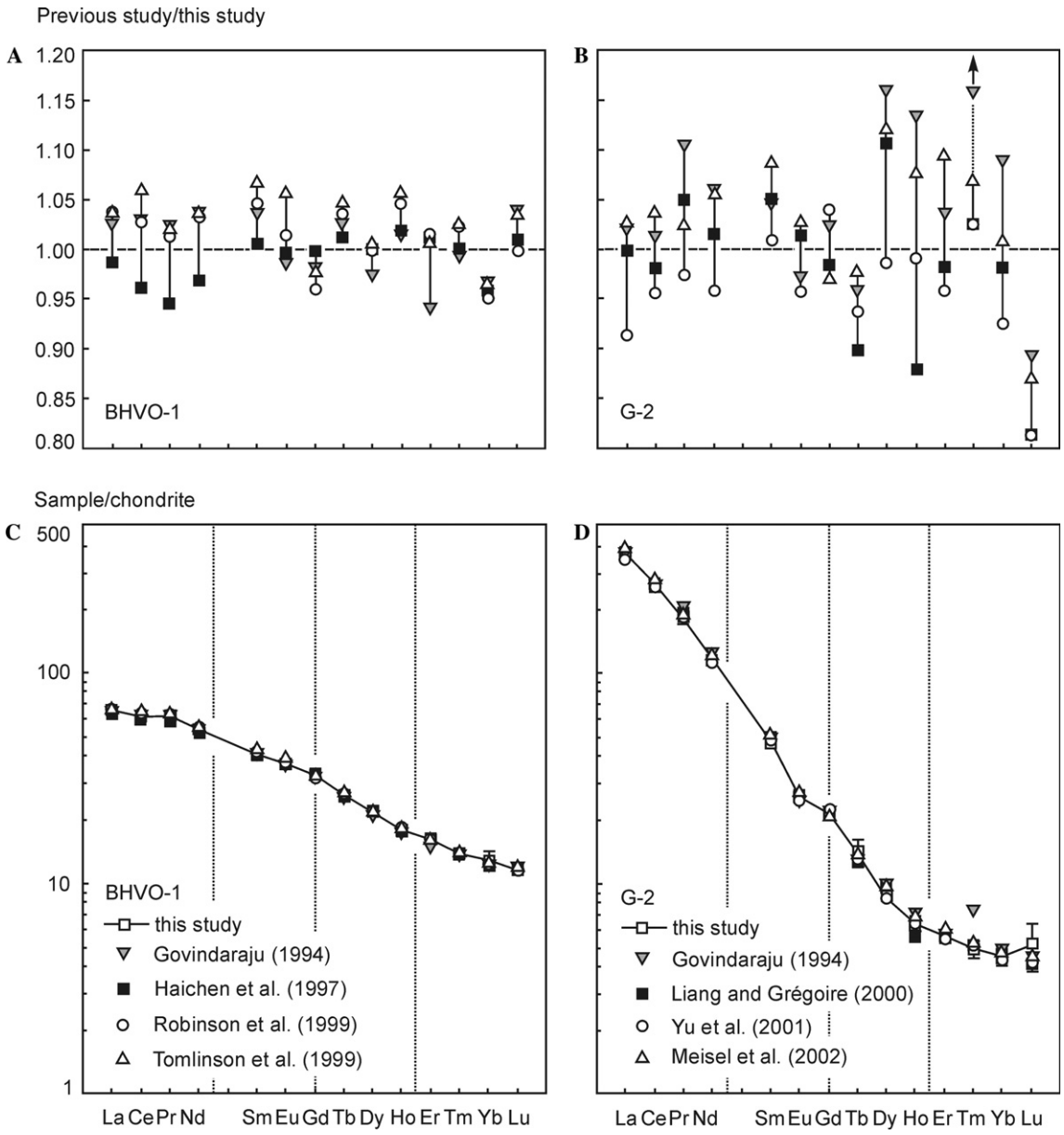

Fig. A2. Comparison of the REE concentrations of the international reference materials BHVO-1 and G-2 determined in the present study with those given by previous workers. The normalized patterns show that the REE determinations are internally consistent and agree, in general, well with the data given in the literature. The plotted REE concentrations represent the arithmetic mean values derived from repeated independent preparations and measurements of both reference materials. The normalization is based on the chondrite data given by Anders and Grevesse (1989).

of the granite G-2, the Tm information value given by Govindaraju (1994) deviates significantly from the concentration of this element as determined in the present study. However, the Tm content derived in the present study agrees well with ICP-MS measurements of other workers (Table A3).

The reliability of the REE determinations can also be evaluated by inspection of the normalized REE patterns of the reference materials BHVO-1 and G-2 because the lanthanides form a coherent group of elements where anomalous behavior is typically restricted to Ce and Eu. The smooth decrease of the normalized REE patterns from La to Lu (Fig. A2) indicates internal consistency of the data and further supports the assumption that systematic errors were only of minor importance. The shapes of the normalized REE pattern suggest that the Pr and Lu contents have been systematically overestimated in the basalt and the granite, respectively. The REE patterns of both reference materials lack tetrads suggesting that convex curvature of the normalized segments of REE patterns is not a result of systematic errors of the analytical procedure (note that a number of international reference materials show convex tetrads that are not introduced by systematic errors; cf. Kawabe, 1995 and Dulski, 2001).

Table B1
Rare earth element concentrations in the samples from the Zinnwald deposit (all data in ppm)

	La	Ce	Pr	Nd	Sm	Eu	Gd	Tb	Dy	Ho	Er	Tm	Yb	Lu
MGt-53 (Albite granite from the endocontact)														
1	16.7	49.4	5.81	15.1	4.46	0.062	2.90	0.751	5.80	1.20	4.62	1.00	9.07	1.34
2	17.0	50.4	5.76	15.3	4.69	0.055	2.77	0.748	5.66	1.18	4.57	0.981	8.98	1.34
3	16.5	48.4	5.61	14.9	4.42	0.056	2.83	0.757	5.61	1.19	4.55	0.988	8.89	1.36
4	17.0	50.2	5.75	15.0	4.44	0.055	2.75	0.730	5.63	1.16	4.54	0.969	8.83	1.33
5	16.7	49.7	5.65	15.0	4.42	0.056	2.78	0.750	5.72	1.18	4.53	0.979	9.06	1.40
Mean	16.8	49.6	5.72	15.1	4.49	0.057	2.81	0.747	5.68	1.18	4.56	0.983	8.97	1.35
SD	0.2	0.8	0.08	0.2	0.12	0.003	0.06	0.010	0.08	0.01	0.04	0.012	0.11	0.03
%RSD	1.3	1.6	1.5	1.0	2.6	5.2	2.1	1.4	1.4	1.3	0.8	1.2	1.2	2.1
MGr-43 (Greisen from the endocontact)														
1	12.0	36.0	4.12	10.7	3.09	0.011	2.28	0.630	4.86	1.00	3.83	0.857	7.97	1.18
2	11.4	34.3	3.89	10.6	3.04	0.011	2.06	0.594	4.60	0.918	3.60	0.800	7.50	1.11
3	12.1	36.4	4.13	10.9	3.14	0.013	2.18	0.606	4.62	0.952	3.66	0.804	7.49	1.11
4	12.2	36.7	4.21	10.8	3.21	0.013	2.27	0.634	4.89	1.00	3.89	0.856	7.87	1.18
5	11.8	35.9	4.10	10.8	3.06	0.012	2.19	0.605	4.61	0.953	3.66	0.806	7.47	1.12
Mean	11.9	35.9	4.09	10.8	3.11	0.012	2.20	0.614	4.72	0.965	3.73	0.825	7.66	1.14
SD	0.3	0.9	0.12	0.1	0.07	0.001	0.09	0.017	0.15	0.035	0.12	0.029	0.24	0.04
%RSD	2.7	2.6	2.9	1.1	2.2	8.3	4.0	2.8	3.1	3.7	3.3	3.5	3.1	3.2
X-2 (Rhyolite from the exocontact)														
1	21.2	51.0	6.98	27.0	9.24	0.024	10.5	2.28	16.5	3.63	12.1	2.01	14.2	2.10
2	21.4	52.4	7.13	27.4	9.33	0.022	10.9	2.32	16.6	3.66	12.0	1.98	14.1	2.07
3	21.0	51.2	6.98	27.0	9.16	0.023	10.7	2.29	16.4	3.65	12.0	2.03	14.1	2.10
4	21.0	51.1	6.98	26.9	9.12	0.024	10.5	2.26	16.3	3.59	12.0	1.98	13.8	2.04
5	21.0	51.0	7.00	26.9	9.18	0.024	10.4	2.21	16.3	3.57	11.9	2.00	13.9	2.06
Mean	21.1	51.3	7.01	27.0	9.21	0.023	10.6	2.27	16.4	3.62	12.0	2.00	14.0	2.07
SD	0.2	0.6	0.07	0.2	0.08	0.001	0.2	0.04	0.1	0.04	0.1	0.02	0.2	0.03
%RSD	0.8	1.2	0.9	0.8	0.9	3.8	1.9	1.8	0.8	1.1	0.6	1.1	1.2	1.3
L-6a (Rhyolite from the exocontact)														
1	22.3	56.6	7.59	30.1	10.6	0.024	12.6	2.80	19.8	4.22	13.4	2.10	15.0	2.17
2	21.7	55.3	7.50	29.6	10.4	0.026	12.6	2.75	19.6	4.12	13.2	2.13	14.6	2.09
3	22.2	56.1	7.64	29.9	10.6	0.026	12.7	2.76	19.3	4.24	13.5	2.18	14.9	2.15
4	22.0	55.5	7.49	29.5	10.6	0.025	12.6	2.72	19.6	4.23	13.4	2.12	14.7	2.14
5	21.7	54.6	7.42	29.1	10.5	0.018	12.4	2.69	19.2	4.21	13.2	2.13	14.4	2.12
Mean	22.0	55.6	7.53	29.6	10.5	0.024	12.6	2.74	19.5	4.20	13.3	2.13	14.7	2.13
SD	0.3	0.8	0.09	0.4	0.1	0.003	0.1	0.04	0.2	0.05	0.1	0.03	0.2	0.03
%RSD	1.3	1.4	1.2	1.3	0.8	14.1	0.9	1.5	1.3	1.1	1.0	1.4	1.6	1.4
MR-15 (Rhyolite from the exocontact)														
1	54.4	116	13.4	46.7	11.0	0.222	10.4	1.86	11.8	2.37	7.11	1.07	7.32	1.03
2	53.8	113	13.1	46.4	10.9	0.220	10.2	1.84	11.6	2.35	6.93	1.05	7.16	1.03
3	53.9	114	13.4	46.4	10.7	0.198	10.3	1.83	11.3	2.27	6.78	1.06	7.09	0.994
4	55.2	115	13.4	47.0	10.9	0.219	10.2	1.82	11.5	2.33	6.89	1.07	7.20	1.04
5	54.8	115	13.4	47.5	10.8	0.233	10.3	1.86	11.9	2.29	7.01	1.04	7.19	1.04
6	54.2	114	13.4	46.0	11.0	0.221	10.3	1.81	11.4	2.30	6.91	1.06	7.04	1.02
7	54.2	114	13.4	45.9	10.8	0.212	10.3	1.85	11.6	2.32	6.86	1.06	7.19	1.02
8	55.3	115	13.4	47.3	10.9	0.228	10.5	1.86	11.8	2.36	7.01	1.05	7.24	1.02
9	53.9	113	13.2	45.7	10.9	0.222	10.4	1.80	11.6	2.32	6.94	1.09	7.18	1.04
10	54.4	114	13.3	46.0	10.9	0.221	10.2	1.88	11.7	2.31	6.95	1.04	7.08	1.02
Mean	54.4	114	13.3	46.5	10.9	0.220	10.3	1.84	11.6	2.32	6.94	1.06	7.17	1.03
SD	0.5	1	0.1	0.6	0.1	0.009	0.1	0.03	0.2	0.03	0.09	0.02	0.08	0.01
%RSD	1.0	0.8	0.8	1.3	0.8	4.3	1.0	1.4	1.6	1.4	1.3	1.4	1.1	1.4
L-4a (Rhyolite from the exocontact)														
1	64.9	130	15.3	53.2	11.4	0.263	10.4	1.79	11.3	2.31	6.54	0.941	5.90	0.854
2	64.4	130	15.1	53.8	11.6	0.249	10.5	1.86	11.5	2.32	6.60	0.961	5.93	0.849
3	64.6	130	15.1	52.8	11.4	0.260	10.7	1.83	11.4	2.27	6.54	0.964	5.96	0.864
4	64.1	129	15.1	52.6	11.5	0.273	10.6	1.83	11.3	2.31	6.65	0.950	5.93	0.874
5	64.7	130	15.1	52.7	11.5	0.267	10.6	1.82	11.3	2.29	6.63	0.960	5.98	0.855
Mean	64.5	130	15.1	53.0	11.5	0.262	10.6	1.83	11.4	2.30	6.59	0.955	5.94	0.859
SD	0.3	<1	0.1	0.5	0.1	0.009	0.1	0.03	0.1	0.02	0.05	0.010	0.03	0.010
%RSD	0.5	0.3	0.6	0.9	0.7	3.4	1.1	1.4	0.8	0.9	0.8	1.0	0.5	1.2
MR-19 (Rhyolite from the exocontact)														
1	51.6	104	12.3	43.7	9.39	0.339	8.05	1.38	8.47	1.65	4.94	0.772	5.41	0.763

Table B1 (*continued*)

	La	Ce	Pr	Nd	Sm	Eu	Gd	Tb	Dy	Ho	Er	Tm	Yb	Lu
2	52.5	106	12.6	44.6	9.48	0.344	8.44	1.44	9.02	1.76	5.25	0.831	5.75	0.843
3	51.0	103	12.3	43.5	9.31	0.340	8.16	1.39	8.63	1.71	5.15	0.802	5.58	0.810
4	51.3	102	12.4	43.3	9.53	0.351	8.22	1.38	8.68	1.72	5.16	0.810	5.58	0.802
5	51.1	102	12.3	43.5	9.36	0.346	8.21	1.39	8.57	1.73	5.14	0.778	5.59	0.813
Mean	51.5	103	12.4	43.7	9.41	0.344	8.22	1.40	8.67	1.71	5.13	0.799	5.58	0.806
SD	0.6	2	0.1	0.5	0.09	0.005	0.14	0.03	0.21	0.04	0.11	0.024	0.12	0.029
%RSD	1.2	1.6	1.1	1.2	1.0	1.4	1.7	1.8	2.4	2.4	2.2	3.0	2.2	3.6
MR-14 (Rhyolite from the exocontact)														
1	66.9	136	15.3	53.3	10.8	0.461	9.31	1.55	9.19	1.81	5.25	0.724	4.72	0.665
2	68.0	137	15.6	53.5	10.9	0.457	9.57	1.54	9.40	1.80	5.25	0.733	4.73	0.679
3	68.1	138	15.2	53.5	10.9	0.454	9.45	1.55	9.37	1.81	5.25	0.738	4.70	0.659
4	67.5	137	15.4	53.4	10.8	0.447	9.53	1.54	9.21	1.78	5.15	0.713	4.58	0.673
5	68.0	137	15.4	53.6	10.9	0.450	9.54	1.58	9.25	1.83	5.35	0.731	4.72	0.685
Mean	67.7	137	15.4	53.5	10.9	0.454	9.48	1.55	9.28	1.81	5.25	0.728	4.69	0.672
SD	0.5	1	0.1	0.1	0.1	0.006	0.10	0.02	0.10	0.02	0.07	0.010	0.06	0.010
%RSD	0.7	0.5	1.0	0.2	0.5	1.2	1.1	1.1	1.0	1.0	1.3	1.3	1.3	1.6
L-3 (Rhyolite from the exocontact)														
1	38.2	80.1	10.8	39.4	8.71	0.283	7.50	1.23	7.26	1.39	4.06	0.586	3.79	0.556
2	36.7	77.5	10.3	37.6	8.18	0.263	7.19	1.16	7.13	1.38	3.92	0.568	3.70	0.532
3	37.9	78.2	10.6	38.8	8.56	0.267	7.52	1.20	7.21	1.42	4.01	0.586	3.84	0.559
4	37.8	79.3	10.6	38.7	8.51	0.262	7.52	1.23	7.44	1.44	4.18	0.595	3.90	0.565
5	37.5	78.3	10.6	38.9	8.60	0.273	7.60	1.21	7.39	1.45	4.07	0.586	3.87	0.556
Mean	37.6	78.7	10.6	38.7	8.51	0.270	7.47	1.21	7.29	1.42	4.05	0.584	3.82	0.554
SD	0.6	1.0	0.2	0.7	0.20	0.009	0.16	0.03	0.13	0.03	0.09	0.010	0.08	0.013
%RSD	1.5	1.3	1.7	1.7	2.3	3.2	2.1	2.4	1.8	2.2	2.3	1.7	2.1	2.3

Notes: SD, standard deviation; %RSD, relative standard deviation in %.

Appendix B. Repeated independent preparation and analysis of samples from the Zinnwald deposit

The whole rock samples from the Zinnwald deposit were repeatedly dissolved and analyzed to determine the element and sample specific random and systematic errors of the REE determinations. The results of the 5–10 independent REE determinations are listed in Table B1 along with the respective arithmetic mean values, standard deviations, and relative standard deviations.

Inspection of the data shows that the ICP-MS investigations on the whole rock samples were performed at high precision. Table B1 shows that the calculated relative standard deviations depend on the REE concentrations and the nature of the sample material investigated. The REE contents in the granite and greisen samples were determined at a precision of 0.8–4.0%RSD at concentrations exceeding 1.0 ppm, whereas analytes in the range of 0.1–1.0 ppm could only be determined at 1.2–3.7%RSD. Even higher relative standard deviations were observed for trace ele-

Table A3
Rare earth element concentrations of the reference materials BHVO-1 and G-2 as determined in the present study and by previous workers (all data in ppm)

	BHVO-1					G-2				
	This study ($n = 5$)	Govindaraju (1994)	Haichen et al. (1997)	Robinson et al. (1999)	Tomlinson et al. (1999)	This study ($n = 5$)	Govindaraju (1994)	Liang and Grégoire (2000)	Yu et al. (2001)	Meisel et al. (2002)
La	15.4	15.8	15.2	16	16.0	87.2	89	87.1	79.7	89.6
Ce	37.9	39	36.4	39	40.2	158	160	155	151	164
Pr	5.57	5.7	5.26	5.65	5.7	16.3	18	17.1	15.9	16.7
Nd	24.3	25.2	23.5	25.1	25.1	51.9	55	52.6	49.8	54.8
Sm	5.98	6.2	6.01	6.26	6.39	6.88	7.2	7.22	6.95	7.48
Eu	2.09	2.06	2.08	2.12	2.21	1.44	1.4	1.46	1.38	1.48
Gd	6.52	6.4	6.50	6.26	6.37	4.20	4.3	4.13	4.37	4.08
Tb	0.936	0.96	0.947	0.97	0.98	0.501	0.48	0.45	0.47	0.49
Dy	5.34	5.2	5.34	5.34	5.37	2.07	2.4	2.29	2.04	2.32
Ho	0.974	0.99	0.992	1.02	1.03	0.353	0.4	0.31	0.35	0.38
Er	2.55	2.4	2.58	2.59	2.57	0.886	0.92	0.87	0.85	0.97
Tm	0.332	0.33	0.332	0.34	0.34	0.117	(0.18)	0.12	0.12	0.125
Yb	2.09	2.02	2.00	1.99	2.02	0.734	0.8	0.72	0.68	0.74
Lu	0.280	0.291	0.282	0.28	0.29	0.123	0.11	0.10	0.10	0.107

Notes: n, number of analyses; underlined, recommended values; and brackets, information values.

ments having concentrations below 0.1 ppm. At comparable concentration ranges, the REE determinations in the rhyolite samples were typically performed at a slightly better precision. The precision achieved ranges from 0.2–2.4%RSD at concentrations exceeding 1.0 ppm and varies from 1.0–4.3%RSD for concentrations between 0.1 and 1.0 ppm. The highest %RSD values were observed for analytes having concentrations below 0.1 ppm.

References

Anders, E., Grevesse, N., 1989. Abundances of the elements: meteoritic and solar. *Geochim. Cosmochim. Acta* **53**, 197–214.

Bau, M., 1996. Controls on the fractionation of isovalent trace elements in magmatic and aqueous systems: evidence from Y/Ho, Zr/Hf, and lanthanide tetrad effect. *Contrib. Mineral. Petrol.* **123**, 323–333.

Bau, M., 1997. The lanthanide tetrad effect in highly evolved felsic igneous rocks - a reply to the comment by Y. Pan. *Contrib. Mineral. Petrol.* **128**, 409–412.

Breiter, K., 1997. The Teplice rhyolite (Krušné Hory Mts., Czech Republic)—chemical evidence of a multiply exhausted stratified magma chamber. *Bull. Czech Geol. Surv.* **72**, 205–213.

Cocherie, A., Johan, V., Rossi, P., Štemprok, M., 1991. Trace element variations and lanthanide tetrad effect studied in a Variscan lithium albite granite: case of the Cinovec granite (Czechoslovakia) [abstract]. In: Pagel, M., Leroy, J.L. (Eds.), *Source, Transport and Deposition of Metals*. Balkema, pp. 745–749.

Dolejš, D., Štemprok, M., 2001. Magmatic and hydrothermal evolution of Li–F granites: Cínovec and Krásno intrusions, Krušné Hory batholith, Czech Republic. *Bull. Czech Geol. Surv.* **76**, 77–99.

Dostal, J., Chatterjee, A.K., 1995. Origin of topaz-bearing and related peraluminous granites of the Late Devonian Davis Lake pluton, Nova Scotia, Canada: crystal versus fluid fractionation. *Chem. Geol.* **123**, 67–88.

Dulski, P., 1994. Interferences of oxide, hydroxide and chloride analyte species in the determination of rare earth elements in geological samples by inductively coupled plasma-mass spectrometry. *Fresenius J. Anal. Chem.* **350**, 194–203.

Dulski, P., 2001. Reference materials for geochemical studies: new analytical data by ICP-MS and critical discussion of reference values. *Geostand. Newsl.* **25**, 87–125.

Ďurišová, J., Charoy, B., Weisbrod, A., 1979. Fluid inclusion studies in minerals from tin and tungsten deposits in the Krušné Hory mountains (Czechoslovakia). *Bull. Minéral.* **102**, 665–675.

Förster, H.J., 1998. The chemical composition of REE–Y–Th–U-rich accessory minerals in peraluminous granites of the Erzgebirge–Fichtelgebirge region, Germany, Part I: the monazite–(Ce)–brabantite solid solution series. *Am. Mineral.* **83**, 259–272.

Förster, H.J., Tischendorf, G., 1994. The western Erzgebirge–Vogtland granites: implications to the Hercynian magmatism in the Erzgebirge–Fichtelgebirge anticlinorium [abstract]. In: Seltmann, R., Kämpf, H., Möller, P. (Eds.), *Metallogeny of Collisional Orogens Focussed on the Erzgebirge and Comparable Metallogenic Settings*, Czech Geological Survey, pp. 35–48.

Govindaraju, K., 1994. 1994 compilation of working values and sample description for 383 geostandards. *Geostand. Newsl.* **18**, 1–158 (special issue).

Haichen, L., Ying, L., Zhanxia, Z., 1997. Determination of ultra-trace rare earth elements in chondritic meteorites by inductively coupled plasma mass spectrometry. *Spectrochim. Acta* **53**, 1399–1404.

Heinrich, C.A., Günther, D., Audétat, A., Ulrich, T., Frischknecht, R., 1999. Metal fractionation between magmatic brine and vapor, determined by microanalysis of fluid inclusions. *Geology* **27**, 755–758.

Irber, W., 1999. The lanthanide tetrad effect and its correlation with K/Rb, Eu/Eu*, Sr/Eu, Y/Ho, and Zr/Hf of evolving peraluminous granite suites. *Geochim. Cosmochim. Acta* **63**, 489–508.

Jahn, B., Wu, F., Capdevila, R., Martineau, F., Zhao, Z., Wang, Y., 2001. Highly evolved juvenile granites with tetrad REE patterns: the Woduhe and Baerzhe granites from the Great Xing'an Mountains in NE China. *Lithos* **59**, 171–198.

Johan, V., Johan, Z., 1994. Accessory minerals of the Cínovec (Zinnwald) granite cupola, Czech Republic. Part 1: Nb-, Ta- and Ti-bearing oxides. *Mineral. Petrol.* **51**, 323–343.

Kawabe, I., 1995. Tetrad effects and fine structures of REE abundance patterns of granitic and rhyolitic rocks: ICP-AES determinations of REE and Y in eight GSJ reference rocks. *Geochem. J.* **29**, 213–230.

Kempe, U., Goldstein, S., 1997. Eu anomalies, tetrad effect and HREE enrichment in fluorites from Sn deposits: Evidence for two source mixing and phase separation [abstract]. *J. Czech Geol. Soc.* **42**, 37.

Kempe, U., Götze, J., 2002. Cathodoluminescence (CL) behaviour and crystal chemistry of apatite from rare-metal deposits. *Mineral. Mag.* **66**, 151–172.

Kempe, U., Gruner, T., Renno, A.D., Wolf, D., 1997. Hf-rich zircons in rare-metal bearing granites: magmatic or metasomatic origin? [abstract]. In: Papunen, H. (Ed.), *Mineral Deposits: Research and Exploration Where do They Meet?* Balkema, pp. 643–646.

Kempe, U., Wolf, D., Sala, M., 1999. Members of the philipsbornite–florencite and chernovite-xenotime solid solution series in metasomatic altered granites of the Zinnwald tin deposit (Erzgebirge, Germany) [abstract]. *Beih. 1 Eur. J. Mineral.* **11**, 120.

Lee, S.G., Masuda, A., Kim, H.S., 1994. An early Proterozoic leucogranitic gneiss with the REE tetrad phenomenon. *Chem. Geol.* **114**, 59–67.

Liang, Q., Grégoire, D.C., 2000. Determination of trace elements in twenty six Chinese geochemistry reference materials by inductively coupled plasma-mass spectrometry. *Geostand. Newsl.* **24**, 51–63.

Lobin, M., 1986. *Time Sequence and Related Evolution of Permocarbonian Sedimentary Rocks in the Eastern and Central Erzgebirge* [in German]. Unpubl. Ph.D. Thesis Bergakademie Freiberg, 63 p.

Masau, M., Černý, P., Chapman, R., 2000. Dysprosian xenotime-(Y) from the Annie Claim #3 granitic pegmatite, southeastern Manitoba, Canada: evidence of the tetrad effect? *Can. Mineral.* **38**, 899–905.

Masuda, A., Akagi, T., 1989. Lanthanide tetrad effect observed in leucogranites from China. *Geochem. J.* **23**, 245–253.

Masuda, A., Kawakami, O., Dohmoto, Y., Takenaka, T., 1987. Lanthanide tetrad effects in nature: two mutually opposite types, W and M. *Geochem. J.* **21**, 119–124.

McLennan, S.M., 1994. Rare earth element geochemistry and the "tetrad" effect. *Geochim. Cosmochim. Acta* **58**, 2025–2033.

Meisel, T., Schöner, N., Paliulionyte, V., Kahr, E., 2002. Determination of rare earth elements, Y, Th, Zr, Hf, Nb and Ta in geological reference materials G-2, G-3, SCo-1 and WGB-1 by sodium peroxide sintering and inductively coupled plasma-mass spectrometry. *Geostand. Newsl.* **26**, 53–61.

Möller, P., 1998. Eu anomalies in hydrothermal minerals: Kinetic versus thermodynamic interpretation [abstract]. In: Hagni, R.D. (Ed.), *Proceedings of the Ninth Quadrennial IAGOD Symposium*, Schweizerbart'sche Verlagsbuchhandlung, pp. 239–246.

Möller, P., Muecke, G.K., 1984. Significance of europium anomalies in silicate melts and crystal-melt equilibria: a re-evaluation. *Contrib. Mineral. Petrol.* **87**, 242–250.

Monecke, T., Monecke, J., Mönch, W., Kempe, U., 2000. Mathematical analysis of rare earth element patterns of fluorites from the Ehrenfriedersdorf tin deposit, Germany: evidence for a hydrothermal mixing process of lanthanides from two different sources. *Mineral. Petrol.* **70**, 235–256.

Monecke, T., Kempe, U., Monecke, J., Sala, M., Wolf, D., 2002. Tetrad effect in rare earth element distribution patterns: a method of quantification with application to rock and mineral samples from granite-related rare metal deposits. *Geochim. Cosmochim. Acta* **66**, 1185–1196.

Monecke, T., Kempe, U., Monecke, J., 2003. Comment on the paper "W- and M-type tetrad effects in REE patterns for water-rock systems in the Tono uranium deposit, central Japan" by Takahasi, Y., Yoshida,

H., Sato, N., Hama, K., Yusa, Y., Shimizu, H. *Chem. Geol*. **202**, 183–184.

Müller, A., Breiter, K., Seltmann, R., Pécskay, Z., 2005. Quartz and feldspar zoning in the eastern Erzgebirge volcano-plutonic complex (Germany, Czech Republic): evidence of multiple magma mixing. *Lithos* **80**, 201–227.

Münker, C., 1998. Nb/Ta fractionation in a Cambrian arc/back arc system, New Zealand: source constraints and application of refined ICPMS techniques. *Chem. Geol.* **144**, 23–45.

Pälchen, W., 1968. *Geochemistry and petrology of post-collisional magmatites in the Variscan Eastern Erzgebirge*, *Saxony* [in German]. Unpubl. Ph.D. Thesis Bergakademie Freiberg, 142 p.

Pan, Y., 1997. Controls on the fractionation of isovalent trace elements in magmatic and aqueous systems: evidence from Y/Ho, Zr/Hf, and lanthanide tetrad effect–a discussion of the article by M. Bau (1996). *Contrib. Mineral. Petrol.* **128**, 405–408.

Pan, Y., Breaks, F.W., 1997. Rare-earth elements in fluorapatite, Separation Lake area, Ontario: evidence for S-type granite–rare-element pegmatite linkage. *Can. Mineral.* **35**, 659–671.

Peppard, D.F., Mason, G.W., Lewey, S., 1969. A tetrad effect in the liquid–liquid extraction ordering of lanthanides (III). *J. Inorg. Nucl. Chem.* **31**, 2271–2272.

Raimbault, L., Baumer, A., Dubru, M., Benkerrou, C., Croze, V., Zahm, A., 1993. REE fractionation between scheelite and apatite in hydrothermal conditions. *Am. Mineral.* **78**, 1275–1285.

Robinson, P., Townsend, A.T., Yu, Z., Münker, C., 1999. Determination of scandium, yttrium and rare earth elements in rocks by high resolution inductively coupled plasma-mass spectrometry. *Geostand. Newsl.* **23**, 31–46.

Rub, A.K., Štemprok, M., Rub, M.G., 1998. Tantalum mineralization in the apical part of the Cínovec (Zinnwald) granite stock. *Mineral. Petrol.* **63**, 199–222.

Sala, M., 1999. *Geochemical and Mineralogical Investigations on Altered Rocks from the Upper Part of the Zinnwald Deposit*, *Eastern Erzgebirge* [in German]. Unpubl. Ph.D. Thesis TU Bergakademie Freiberg, 96 p.

Seltmann, R., Breiter, K., 1995. Late-Variscan crustal evolution and related tin-tungsten mineralization in the Altenberg-Teplice caldera (eastern Erzgebirge). In: Breiter, K., Seltmann, R. (Eds.), *Ore Mineralizations of the Krušné Hory Mts (Erzgebirge)*, Czech Geological Survey, pp. 65–76.

Seltmann, R., Breiter, K., Schilka, W., Benek, R., 1996. The Altenberg-Teplice caldera: reversed zonation of a stratified magma chamber [abstract]. In: Lippolt, H.J. et al. (Eds.), *V.M. Goldschmidt Conference Heidelberg. Journal of Conference Abstracts*, Cambridge Publications, p. 556.

Seltmann, R., Förster, H.J., Gottesmann, B., Sala, M., Wolf, D., Štemprok, M., 1998. The Zinnwald greisen deposit related to post-collisional A-type silicic magmatism in the Variscan eastern Erzgebirge/Krušné Hory. In: Breiter, K. (Ed.), *Genetic Significance of Phosphorus in Fractionated Granites. Excursion Guide International Conference IGCP Project 373 in Perslak*, Czech Geological Survey, pp. 33–50.

Štemprok, M., 1967. The origin of tin-tungsten mineralization in the Erzgebirge [in German]. *Mineral. Deposita* **2**, 102–118.

Štemprok, M., Šulcek, Z., 1969. Geochemical profile through an ore-bearing lithium granite. *Econ. Geol.* **64**, 392–404.

Štemprok, M., Seltmann, R., Breiter, K., 1995. The Cínovec/Zinnwald Sn-W-Li deposit. In: Breiter, K., Seltmann, R. (Eds.), *Ore Mineralizations of the Krušné Hory Mts (Erzgebirge)*, Czech Geological Survey, pp. 77–83.

Štemprok, M., Holub, F.V., Novák, J.K., 2003. Multiple magmatic pulses of the eastern volcano-plutonic complex, Krušné Hory/Erzgebirge batholith, and their phosphorus contents. *Bull. Geosci.* **78**, 277–296.

Takahashi, T., Kawabe, I., 2003. Lanthanide tetrad effects in Naegi granite and pegmatite, central Japan [abstract]. *Geochim. Cosmochim. Acta* **67** (Suppl.), A469.

Takahashi, Y., Yoshida, H., Sato, N., Hama, K., Yusa, Y., Shimizu, H., 2002. W- and M-type tetrad effects in REE patterns for water-rock systems in the Tono uranium deposit, central Japan. *Chem. Geol.* **184**, 311–335.

Takahashi, Y., Amano, K., Hama, K., Mizuno, T., Yoshida, H., Shimizu, H., 2003. Reply to the comment by T. Monecke, U. Kempe and J. Monecke on "W- and M-type tetrad effects in REE patterns for water–rock systems in the Tono uranium deposit, central Japan". *Chem. Geol.* **202**, 185–189.

Thomas, R., Förster, H.J., Rickers, K., Webster, J.D., 2005. Formation of extremely F-rich hydrous melt fractions and hydrothermal fluids during differentiation of highly evolved tin-granite magmas: a melt/fluid-inclusion study. *Contrib. Mineral. Petrol.* **148**, 582–601.

Tomlinson, K.Y., Hughes, D.J., Thurston, P.C., Hall, R.P., 1999. Plume magmatism and crustal growth at 2.9 to 3.0 Ga in the Steep Rock and Lumby Lake area, western Superior Province. *Lithos* **46**, 103–136.

Veksler, I.V., Dorfman, A.M., Kamenetsky, M., Dulski, P., Dingwell, D.B., 2005. Partitioning of lanthanides and Y between immiscible silicate and fluoride melts, fluorite and cryolite and the origin of the lanthanide tetrad effect in igneous rocks. *Geochim. Cosmochim. Acta* **69**, 2847–2860.

Webster, J., Thomas, R., Förster, H.J., Seltmann, R., Tappen, C., 2004. Geochemical evolution of halogen-enriched granite magmas and mineralizing fluids of the Zinnwald tin-tungsten mining district, Erzgebirge, Germany. *Mineral. Deposita* **39**, 452–472.

Wolf, L., 1960. Drilling the coal occurrence at Schönfeld, eastern Erzgebirge [in German]. *Z. Angew. Geol.* **6**, 341–344.

Wolf, D., Rene, M., Kempe, U., 2002. New occurrences of brabandite in Sn-granites of the Erzgebirge and the Slavkovsky les [in German, abstract]. *Beih. 1 Eur. J. Mineral.* **14**, 177.

Wood, S.A., 2003. The geochemistry of rare earth elements and yttrium in geothermal waters. *SEG Spec. Pub.* **10**, 133–158.

Yu, Z., Robinson, P., McGoldrick, P., 2001. An evaluation of methods for the chemical decomposition of geological materials for trace element determination using ICP-MS. *Geostand. Newsl.* **25**, 199–217.

Yurimoto, H., Duke, E.F., Papike, J.J., Shearer, C.K., 1990. Are discontinuous chondrite-normalized REE patterns in pegmatitic granite systems the results of monazite fractionation? *Geochim. Cosmochim. Acta* **54**, 2141–2145.

Zhao, J.X., Cooper, J.A., 1993. Fractionation of monazite in the development of V-shaped REE patterns in leucogranite systems: evidence from a muscovite leucogranite body in central Australia. *Lithos* **30**, 23–32.